Classical nonlinear response of a chaotic system. I. Collective resonances

Sergey V. Malinin and Vladimir Y. Chernyak*
Department of Chemistry, Wayne State University, 5101 Cass Avenue, Detroit, Michigan 48202, USA
(Received 30 January 2008; published 7 May 2008)

We develop a general semiquantitative picture of nonlinear classical response in strongly chaotic systems. In contrast to behavior in integrable or almost integrable systems, the nonlinear classical response in chaotic systems vanishes at long times. The exponential decay of the response functions in the case of strong chaos is attributed to both exponentially decaying and growing elements in the stability matrices. We calculate the linear and second-order response in one of the simplest chaotic systems: free classical motion on a compact surface of constant negative curvature. The response reveals certain features of collective resonances which do not correspond to any periodic classical trajectories. We demonstrate the relevance of the model for the interpretation of spectroscopic experiments.

DOI: 10.1103/PhysRevE.77.056201 PACS number(s): 05.45.Ac, 78.20.Bh, 61.20.Lc, 02.40.−k

I. INTRODUCTION

Time-resolved femtosecond spectroscopy constitutes a powerful tool that probes electronic and vibrational coherent dynamics of complex molecular systems in condensed phases [1–6]. Spectroscopic techniques allow for direct measurements of the time- and frequency-domain optical response functions that carry detailed information on the underlying dynamical phenomena. Nonlinear spectroscopy contains additional information on nonequilibrium processes absent in linear measurements.

In complex systems, such as polyatomic molecules, vibrational dynamics of many degrees of freedom can be adequately described by using semiclassical and classical approaches. In particular, at sufficiently high energies the complexity often originates from strongly anharmonic motion which can be treated classically [7].

A number of studies have been devoted to the nonlinear response in integrable dynamical systems [8–12]. Classical nonlinear response functions have been shown to diverge with time in the general case [12], although in certain cases the divergence can be removed by thermal averaging using the canonical distribution [8,9]. The latter effect can be viewed as a result of destructive interference of different paths (dephasing), while the divergence is associated with the rephasing.

The divergence would pose a major problem for the whole concept of perturbative response. On the other hand, quantum response functions do not exhibit any divergences. However, application of the fully quantum description is often unmanageable in the systems of interest. It has been demonstrated that systematic $\hbar$ expansion cures the divergence when the limit of vanishing $\hbar$ is taken after obtaining the asymptotics of long times [10,11]. Alternatively the divergence can be removed by adding noise that models interaction with a bath [13].

However, stable (integrable) dynamics is only characteristic of situations close to equilibrium. At higher energies, as anharmonicity sets in, a typical situation corresponds to dynamical behavior with chaotic features [14]. Although the most generic dynamical system has a mixed phase space (with both regular and chaotic regions), the unstable (hyperbolic) dynamics may be more common due to the stability of chaos with respect to perturbations [14–17]. The motion can be completely chaotic for higher temperatures or in essentially nonequilibrium processes such as photoinduced molecular dynamics on the excited electronic adiabatic surfaces [18].

In integrable systems the classical nonlinear response diverges because some elements of the stability matrix (Jacobian matrix in terms of the phase-space variables) linearly grow with time [10]. In the chaotic case, a much stronger—exponential—growth of the matrix elements has naturally raised more doubts about the validity of the classical response formalism [19].

The situation is much better understood for the case of the linear response. A strongly chaotic system is characterized by a special spectrum of the Liouville operator [20–22]. The spectrum consists of complex Ruelle-Pollicott (RP) resonances whose real and imaginary parts determine the decay and oscillations of the correlations. A long-time decay of correlations slower than exponential occurs in systems with "weaker" chaos (e.g., nonuniformly hyperbolic systems) and is attributed to a gapless spectrum. In any case, the asymptotic decay of correlations in chaotic systems seems quite natural. Physical phase-space distributions (or even singular distribution after physically meaningful coarse graining) behave in agreement with our intuition: they rapidly approach equilibrium (or a stationary state). As we know from the analog [23] of the fluctuation-dissipation theorem (FDT), the linear response is simply related to the two-point correlation and thus exhibits the expected decaying behavior. The validity of the linear response theory and generalized FDT relations for finite perturbations (which are particularly important in chaotic systems) have been extensively studied (see, for example, Refs. [24–27]).

In fact, the behavior of two-point correlations in strongly chaotic (uniformly hyperbolic) systems is so well understood that some readers might wonder why we do not simply carry over this understanding to the nonlinear response. A reason for this question might be a relatively rare occurrence of the nonlinear response beyond the spectroscopic community. It

*chernyak@chem.wayne.edu

is well known [23,28] that a nonlinear response function cannot be simply reduced to the correlation functions and necessarily contains the information about the evolution of small deviations, formally represented by the stability matrices. A numerical analysis [29] confirmed the convergence of the classical nonlinear response for chaotic dynamics. In spite of its apparent importance, to the best of our knowledge, the problem of the nonlinear response in chaotic systems has never been addressed by analytical methods (however, see Ref. [30] and references therein). We note that analytical calculations of the response are rarely feasible in nonintegrable systems, whereas numerical simulations are complicated by the exponential divergence of the stability matrices.

A brief summary of our results can be found in Ref. [31]. The present paper is the first part of the series. Here we show that (i) the classical linear and nonlinear responses of a strongly chaotic system exhibit decay and oscillations as a function of times between the driving pulses, and (ii) the Fourier transform of the two-dimensional (2D) second-order response function reveals broad and asymmetric peaks that can be viewed as signatures of chaos in the underlying dynamics.

The paper is organized as follows. In Sec. II we review the classical response theory using the Liouville representation of classical mechanics. In Sec. III we establish a general semiquantitative picture of the linear and nonlinear response functions and show that in the case of strong chaos they exponentially decay at long times. To exemplify our arguments, in Sec. IV we consider a chaotic model of free motion on a compact surface of constant negative curvature. This model (also referred to as Hadamard-Gutzwiller model), which constitutes a well-known example of classical chaos and a prototype for quantum chaos, allows for an analytical treatment due to strong dynamical symmetry. In Sec. V we present our calculation of the second-order nonlinear response function. We derive recurrence relations for the matrix elements of the dipole and formulate a resummation method for the resulting sign alternating series. This enables us both to derive an asymptotic expansion and to develop an efficient numerical procedure for the second-order response function. This calculation constitutes the main technical result of the paper. The results of numerical evaluation of 2D spectroscopic signals are presented in Sec. VI. All necessary technical details are summarized in the Appendixes.

In the following paper [32] of the series we regularize the spectral decomposition of the response by introducing an infinitesimal noise to the classical dynamics.

II. CLASSICAL RESPONSE IN LIOUVILLE SPACE

In this section we review a general formalism of the classical response theory, using the language of probability distributions (see, e.g., Ref. [29]). We adopt the Liouville picture of classical mechanics where the system state is described by a time-dependent distribution $\rho(\boldsymbol{\eta},t)$, whereas the observables are represented by functions of phase-space variables $\boldsymbol{\eta}$. This language is especially advantageous in a chaotic case, where individual trajectories do not provide meaningful information on the system relaxation.

Consider classical Hamiltonian dynamics that occurs in the phase space M equipped with a Poisson bracket. Evolution of a system, driven by an external time-dependent uniform field $\mathcal{E}(t)$, is described by the classical Liouville equation with a time-dependent Hamiltonian $H_T(t)$:

$$\frac{\partial \rho(\boldsymbol{\eta},t)}{\partial t} = -\hat{L}_T(t)\rho(\boldsymbol{\eta},t), \tag{1}$$

$$\hat{L}_T(t)\cdots = \{H_T(t),\ldots\}, \quad H_T(t) = H - \mathcal{E}(t)f, \tag{2}$$

where $H(\boldsymbol{\eta})$ is the time-independent Hamiltonian of the free system, and the dipole moment (polarization) $f(\boldsymbol{\eta})$ describes the coupling of the system to the driving field. The choice of the sign in the Poisson brackets $\{\ldots,\ldots\}$ corresponds to the expression $\dot{\boldsymbol{\eta}}=\hat{L}\boldsymbol{\eta}$ of the phase-space velocity in the unperturbed system in terms of the Liouville operator

$$\hat{L}\cdots = \{H,\ldots\}. \tag{3}$$

In many cases $f(\boldsymbol{\eta})$ is also an observable (e.g., polarization) that creates spectroscopic signals; therefore the measured value is given by the time-dependent average

$$\langle f(\boldsymbol{\eta}(t))\rangle = \int d\boldsymbol{\eta}\, \rho(\boldsymbol{\eta},t) f(\boldsymbol{\eta}). \tag{4}$$

The undriven system with Hamiltonian H is characterized by the equilibrium distribution $\rho_0(\boldsymbol{\eta})$ which depends only on the conserved energy $E=H(\boldsymbol{\eta})=$const of the system, i.e., $\{H,\rho_0\}=0$. The average of f for the equilibrium distribution $\rho_0(\boldsymbol{\eta})$ normally vanishes (in spectroscopic literature this is often referred to as the absence of the permanent dipole):

$$\int d\boldsymbol{\eta}\, \rho_0(\boldsymbol{\eta}) f(\boldsymbol{\eta}) = 0. \tag{5}$$

The response theory is based on a perturbative expansion of the measured signal in powers of the driving field. The response functions can be naturally obtained by calculating corrections to the density distribution. We start by solving the equation

$$(\partial_t + \hat{L})\rho_1 = \mathcal{E}(t)\{f,\rho_0\}, \tag{6}$$

to get the linear-in-$\mathcal{E}$ correction to the initial (equilibrium) density distribution:

$$\rho_1(t) = \int_0^t d\tau_1 \mathcal{E}(\tau_1) e^{-\hat{L}(t-\tau_1)}\{f,\rho_0\}. \tag{7}$$

The corrections to ρ_0 in all orders of $\mathcal{E}$ can be obtained by solving equations similar to Eq. (6) and result in an expansion $\rho=\rho_0+\rho_1+\cdots$ where ρ_n represents the contribution of nth order in the field $\mathcal{E}$. This leads to a natural representation of the observable in the form of the expansion

$$\langle f\rangle \equiv \int d\boldsymbol{\eta}\, \rho(\boldsymbol{\eta},t) f(\boldsymbol{\eta}) \tag{8}$$

$$= \int_0^t d\tau_1 S_1(t;\tau_1)\mathcal{E}(\tau_1) + \int_0^t d\tau_2 \int_0^{\tau_2} d\tau_1 S_2(t;\tau_1,\tau_2)\mathcal{E}(\tau_1)\mathcal{E}(\tau_2) + \cdots, \tag{9}$$

which defines the response functions $S_n(t;\ldots,\tau_1)$. The response function of order n depends on $n+1$ time variables, which can be reduced to n time intervals $t_n=t-\tau_n,\ldots,t_1=\tau_2-\tau_1$ when the unperturbed dynamics has no explicit time dependence. In the time interval representation, the linear and second-order response functions read

$$S^{(1)}(t_1) = \int d\boldsymbol{\eta}\, f(\boldsymbol{\eta}) e^{-\hat{L}t_1}\{f(\boldsymbol{\eta}),\rho_0\}, \tag{10}$$

$$S^{(2)}(t_1,t_2) = \int d\boldsymbol{\eta}\, f(\boldsymbol{\eta}) e^{-\hat{L}t_2}\{f(\boldsymbol{\eta}), e^{-\hat{L}t_1}\{f(\boldsymbol{\eta}),\rho_0\}\}. \tag{11}$$

The expressions for the response functions have a simple interpretation: each Poisson bracket with the dipole corresponds to an interaction with the driving field; the evolution operators propagate the perturbations; the observable is found as the average of the polarization operator in the perturbed system. The appearance of the second Poisson bracket in the formula for the second-order response prevents its expression in terms of the correlation function with the help of the FDT analog [23,28]. We focus on the case when the dipole and polarization operators coincide, although a more general situation is only slightly more complicated. The expressions (10) and (11) will be the starting point of a general semiquantitative analysis of response functions in strongly chaotic systems as well as a detailed calculation for a particular chaotic system.

III. QUALITATIVE PICTURE OF RESPONSE IN A HYPERBOLIC DYNAMICAL SYSTEM

A. Chaotic dynamics

Integrable and almost integrable Hamiltonian dynamics reviewed in Appendix A is typical for low energies when the system is in the neighborhood of a stable stationary point (close to equilibrium).

In this section we present a semiquantitative picture of nonlinear response in strongly chaotic systems. Due to the analog of the FDT, the stability matrices affect the response functions starting only with the second order [23,29]. The divergence of the nonlinear response functions in the integrable case can be attributed to the growth with time of certain stability matrix components. In the case of strong chaos there are components of the stability matrices that grow exponentially $\sim e^{\lambda t}$ with time, λ being the Lyapunov exponent. Nevertheless, numerical simulations have demonstrated that at least for some examples of chaotic dynamical systems the classical nonlinear response functions are free of unphysical divergences [29].

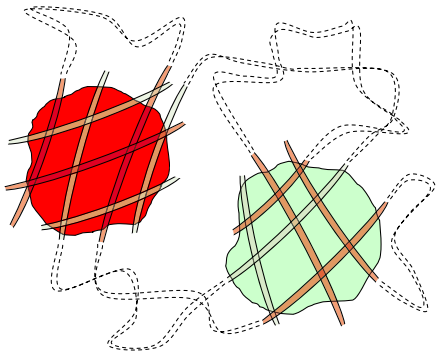

FIG. 1. (Color online) Schematic picture of the cross section of the phase space along the surface defined by the stable and unstable directions. Initial distribution of f is presented by two oppositely charged regions (dark red and light green). As time elapses the distributions elongate along unstable directions and contract along stable ones.

Below we consider strongly chaotic Hamiltonian systems known as uniformly hyperbolic or Smale flows (for a review see Refs. [14–17]). In these systems with the $2n$-dimensional phase space at all points of the $(2n-1)$-dimensional energy shell, or all relevant points (the relevant points belong to the so-called nonwandering subset) in the Smale case, one can define n_+ unstable and n_- stable tangent directions with $n_+ + n_- = 2n-2$, so that a small deviation from a trajectory along the stable (unstable) directions decays exponentially in time for forward (backward) dynamics. The stable (unstable) directions can be locally integrated to obtain stable (unstable) manifolds of dimension n_- (n_+). Note that n_+ (n_-) is the number of positive (negative) Lyapunov exponents. Also note that in the case of Hamiltonian dynamics the phase-space volume is conserved so that all Lyapunov exponents sum up to zero,

$$\lambda \equiv \sum_{j=1}^{n_+} \lambda_j^{(+)} = -\sum_{j=1}^{n_-} \lambda_j^{(-)}. \tag{12}$$

We will consider the simplest case of the lowest dimension $n=2$ of the coordinate space that allows for chaotic dynamics. The isoenergetic shell is three-dimensional; therefore, we have $n_+=n_-=1$, and two nontrivial Lyapunov exponents $\pm\lambda$.

A schematic picture of the linear and second-order response formation in a hyperbolic chaotic system is shown in Fig. 1. We start with the linear response function $S^{(1)}(t)$. Since the equilibrium distribution depends on the system energy only, we can recast the expression for the linear response [Eq. (10)] using the FDT analog:

$$S^{(1)}(t) = \partial_t I^{(1)}(t) = \partial_t \int d\boldsymbol{\eta}\, f e^{-\hat{L}t} f \partial_E \rho_0, \tag{13}$$

where E is the energy. Since $\int d\boldsymbol{x}\, f=0$ (no permanent dipole), we can consider the simplest setup when the function f is represented by two small separate regions in the phase space where it adopts positive and negative values (an extension of our arguments to the general case is straightforward). By our assumption, the linear sizes of the regions $a \ll l$ are small

compared to the linear size l of the compact phase space. Evolution during time t changes the shapes of the regions. In the case of hyperbolic dynamics for $t \gg 1$, the shape becomes similar to ribbonlike fettuccine: elongated along the unstable direction by a factor $e^{\lambda t}$, narrowed along the stable one by $e^{-\lambda t}$ (we reiterate that λ is the positive Lyapunov exponent), and unchanged along the flow. The long ribbon becomes evenly folded in the entire accessible energy shell. The overlap of the distributions f and $e^{-\hat{L}t} f \partial_E \rho_0$ in Eq. (13) is represented by a large number $N_1(t)$ of disconnected regions. The dimensions of each region are typically a, $ae^{-\lambda t}$, and a along the flow, in the stable and unstable directions, respectively. This gives the volume of the single 3D region in the energy shell, $v_1(t) \sim a^3 e^{-\lambda t}$. A typical distance $d(t)$ between the fettuccine ribbons in the overlap regions can be easily estimated as $d(t) \sim l^3 a^{-2} e^{-\lambda t}$, which corresponds to

$$N_1(t) \sim (a/l)^3 e^{\lambda t} \tag{14}$$

disconnected regions of the overlap. Since f assumes opposite signs in the two initial regions, the distribution $e^{-\hat{L}t} f \partial_E \rho_0$ consists of two positively and negatively "charged" fettuccine. The cancellations among the overlap contributions result in a signal determined by a typical fluctuation proportional to $\sqrt{N_1}$, and the overlap integral attains a factor $\sqrt{N_1} v_1$. This results in the decaying long-time asymptotic of the linear response function $S^{(1)}(t) \sim e^{-\lambda t/2}$.

We are now in a position to consider the second-order response function $S^{(2)}(t_1, t_2)$. Propagating the observable f in Eq. (11) backward in time, we interpret the second-order response as an overlap

$$S^{(2)}(t_1, t_2) = \partial_{t_1} I^{(2)}(t_1, t_2) = \partial_{t_1} \int d\boldsymbol{\eta}\, f_- \xi^j \partial_j f_+ \tag{15}$$

of the distributions $f_-(\boldsymbol{\eta}) = \exp(\hat{L} t_2) f$ and $\xi^j \partial_j f_+(\boldsymbol{\eta})$ with $f_+ = \exp(-\hat{L} t_1) f \partial_E \rho_0$ and the vector field $\xi^j \partial_j = \{f, \cdot\}$. Similar to the case of linear response for $t \gg 1$, the shapes of both distributions $f_\pm(\boldsymbol{\eta})$ become similar to ribbonlike fettuccine, unchanged along the flow. Since f_- results from reverse dynamics, the distributions f_+ and f_- are elongated along the unstable and stable directions of the positive time evolution, by the factors $e^{\lambda t_1}$ and $e^{\lambda t_2}$, respectively. Each of the distributions f_- and f_+ consists of two positively and negatively charged fettuccine originating from two oppositely signed separate regions of dipole moment distribution f. Since the vector field $\boldsymbol{\xi}$ introduced earlier is zero outside the support of f, the integration in Eq. (15) is restricted to the overlap of three distributions: f and $f_\pm$. The overlap of each of the distributions f_+ and f_- with f is represented by $N_1(t_1)$ and $N_1(t_2)$ disconnected fettuccine pieces as found in Eq. (14). Therefore the overlap of all three distributions is represented by $N_2(t_1, t_2) \sim N_1(t_1) N_1(t_2) \sim (l/a)^6 e^{-\lambda(t_1+t_2)}$ disconnected regions. The linear dimensions of each disconnected region in the stable, unstable, and flow directions are estimated as $ae^{-\lambda t_1}$, $ae^{-\lambda t_2}$, and a, respectively. Therefore the volume of each disconnected region is $v_2(t) \sim a^3 e^{-\lambda(t_1+t_2)}$.

If instead of the second-order response function we were dealing with a three-point correlation function, the rest of the story would be straightforward. The three-point correlation function has the form of the overlap integral $I^{(2)}(t_1, t_2)$ if the differential operator $\xi^j \partial_j = \{f, \cdot\}$ is replaced by the operator for multiplying by $f(\boldsymbol{\eta})$. In full analogy with the linear response case, cancellations of oppositely signed contributions of similar magnitudes result in a factor $\sqrt{N_2 v_2} \sim e^{-\lambda(t_1+t_2)/2}$, which shows a typical long-time decay of the three-point correlation function. The situation with the nonlinear response function is apparently more complicated, since the vector field $\boldsymbol{\xi}$ generally has a component along the stable direction, and thus the term $\xi^j \partial_j f_+$ may create an exponentially large factor proportional to $e^{\lambda t_1}$. This is the Liouville space signature of the exponentially growing components of the stability matrix, which affects the response starting at second order due to FDT [23,29]. The exponentially growing components of the stability matrix could have caused an exponential divergence of the nonlinear response, since the interaction with the driving field can be considered as a kick leading to an infinitesimal deviation that grows exponentially with time. This would actually happen if the initial distribution was δ-functional concentrated at some point in phase space, and the signal was measured by a deviation of the perturbed trajectory from its unperturbed counterpart. However, the dipole f that describes the system coupling to the driving field is represented by a smooth function. As shown below, because of this smoothness the exponentially diverging terms cancel out completely. This demonstrates that response in chaotic systems should be treated by using the Liouville (distribution-based) representation of classical dynamics, while its dual trajectory-based picture may be misleading.

To prove the harmlessness of the derivative in the second-order response function, we decompose the vector field $\boldsymbol{\xi} = \boldsymbol{\xi}_E + \boldsymbol{\xi}_0 + \boldsymbol{\xi}_+ + \boldsymbol{\xi}_-$ into the components along the energy, flow, unstable, and stable directions. This leads to a natural decomposition of the overlap integral, according to Eq. (15):

$$I^{(2)} = I_E^{(2)} + I_0^{(2)} + I_+^{(2)} + I_-^{(2)}. \tag{16}$$

The term $I_+^{(2)}$ involves a derivative along the stable direction which provides an additional exponentially small $e^{-\lambda t_1}$ factor, since the distribution f_+ is elongated along the unstable direction. The dangerous term that involves derivatives along the sharp feature is represented by $I_-^{(2)}$. The aforementioned cancellation can be seen after the integration by parts:

$$I_-^{(2)} = -\int d\boldsymbol{\eta}\, \mathrm{div}\boldsymbol{\xi}_- f_- f_+ - \int d\boldsymbol{\eta}\, f_+ \xi_-^j \partial_j f_-. \tag{17}$$

The first term in Eq. (17) includes the time-independent distribution $\mathrm{div}\boldsymbol{\xi}_-$. The second term contains the derivative in the stable direction of the distribution f_-. Therefore, it acquires an additional exponentially small factor $e^{-\lambda t_2}$ and becomes negligible at long times. Finally, at long times we have

$$I^{(2)} \approx \int d\eta\, f_-(-\mathrm{div}\boldsymbol{\xi}_- + \xi_0^j\partial_j + \xi_E^j\partial_j)f_+. \qquad (18)$$

The terms in Eq. (18) do not include derivatives that can provide exponentially growing or decaying factors. Therefore, according to the arguments presented above, the second-order response function has a long-time asymptotic $S^{(2)}(t_1,t_2)\sim e^{-\lambda(t_1+t_2)/2}$ similar to the three-point correlation function. Stated differently, the exponentially growing components of the stability matrices, which in principle enter the expressions for nonlinear response functions [23,29], do not affect the long-time behavior of the nonlinear response, due to the smoothness of the dipole function $f(\boldsymbol{\eta})$.

We can extend the semiquantitative arguments developed for the Hamiltonian chaos with the lowest possible number $n=2$ of degrees of freedom to a general case $n\geq 2$ in a straightforward way. This leads to the same asymptotic expressions for the magnitudes of the response functions $|S^{(1)}(t)|\sim e^{-\lambda t/2}$ and $|S^{(2)}(t_1,t_2)|\sim e^{-\lambda(t_1+t_2)/2}$, where λ should be interpreted in the sense of Eq. (12) as the sum of positive Lyapunov exponents. The same approach also allows one to estimate the response functions of higher orders and find their exponential decay in a similar form. Although we focus on the autoresponse functions (when the coupling to the driving field and the observable are represented by the same operator), the above analysis applies to a more general situation as well, thanks to the chaotic mixing.

We emphasize that the above estimates are valid for strong chaos. It is well known [33] that in some chaotic systems the correlations decay as a power law rather than exponentially. Such chaotic systems are distinguished because of the nonuniform expansion rate. A flow is defined to be uniformly hyperbolic if the stable and unstable directions span the space of linearized deviations transverse to the flow, whereas all the expansion and contraction rates are bounded away from zero uniformly (i.e., the bounds are trajectory independent) for almost all trajectories.

Nonuniformly hyperbolic chaotic systems are also referred to as marginally unstable. They are close to the systems with mixed phase space, which contains both chaotic and integrable regions: the origin of their peculiar behavior is the sticking of trajectories to certain regions of phase space. If the system spends a long enough time in the vicinity of these regions, the resulting behavior my lead to a decay of correlations which is slower than exponential. For instance, in the stadium billiard, the parallel trajectories do not diverge at all while bouncing between the straight sides; an interplay between the measure of the trajectories with a small reflection angle and the time during which the local integrability persists results in the power law decay of correlations [34]. The exponential decay of correlations in a hard-sphere gas, another nonuniformly hyperbolic system, has a rate different from the mixing rate [35]. The linear response function must show the same behavior as correlations due to FDT relations. The asymptotic behavior of the nonlinear response might be similar because, as proven below, it is also controlled by the spectrum of Ruelle-Pollicott resonances, which turns out to be gapless in marginally unstable systems.

Throughout the paper we intend the term "strongly chaotic" to mean "uniformly hyperbolic."

B. Effective negative curvature of configuration space

In Sec. III A we have established a semiquantitative picture of response in classical systems with uniformly hyperbolic dynamics. In the forthcoming sections we support these arguments by performing explicit analytical calculations in a model system of a free particle on a compact Riemann surface of constant negative curvature. Here we present a rationale why this simple model system can be viewed as a representative example that bears the basic qualitative features of chaotic dynamics in a molecule or a molecular ensemble at high enough energies.

First of all, classical motion of a molecular system is equivalent to motion of a multidimensional particle in a potential $U(\boldsymbol{r})$, where $\boldsymbol{r}$ stands for a complete set of nuclear coordinates. Trajectories of a particle with energy E in arbitrary potential $U(\boldsymbol{r})$ are known to be the same as for a free motion in a curved space with the metric $g_{ik}=[1-U(\boldsymbol{r})/E]\delta_{ik}$ [14,15,37]. Although the potential generates nonuniform motion along the trajectories, the dominant feature of the dynamics is the exponentially growing separation between the trajectories in the regions where the metric curvature is negative. The regions of the configuration space that correspond to negative curvature work as defocusing lenses, causing instability, i.e., divergence of close trajectories. For example, close trajectories diverge every time they approach the boundary of the classically inaccessible island or pass a region of a potential local maximum that belongs to the accessible region. Passage through the stable regions with positive curvature is often unable to compensate for the instability, since the stability causes oscillatory rather than converging behavior (the trajectories diverge after the initial focusing). The resulting dynamics is not necessarily strongly chaotic but the chaotic regions can play a remarkable role even in the behavior of a system with the mixed phase space [36]. Moreover, the chaos may also be caused by the positive but inhomogeneous curvature [37] of the configuration space.

In addition, when the motion is finite, the accessible part of the configuration space at a given energy can be multiply connected. In the simplest $n=2$ case of two coordinates the motion occurs inside a disklike region punctured by g forbidden islands (see Fig. 2). Boundaries of the accessible area are represented by curved lines where the potential energy $U(\boldsymbol{r})$ coincides with the total energy E. Some fraction of trajectories approaches the boundaries so close that this can be qualified as reflection. Using Sinai's argument [15,38], we can interpret the reflection as continuing motion on the antipode replica of the accessible region glued to its original via the boundaries. The resulting compact surface has the topology of a sphere with g handles (Riemann surface of genus g). According to the Gauss-Bonnet theorem, in the $g>1$ case the average Gaussian curvature is negative, which implies regions of instability and results in unstable (hyperbolic) dynamics.

We also note that a loose distinction between reflected and deflected trajectories that approach the boundaries should not

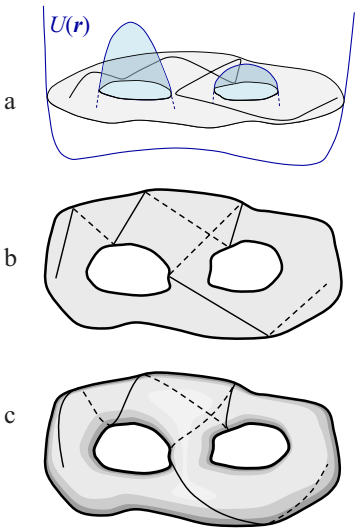

FIG. 2. (Color online) From the motion in a potential to the motion on a compact surface. (a) For fixed particle energy E, a potential with several maxima defines the multiply connected classically allowed region. (b) Idealization of the hard-wall potential: Trajectories are confined within the original classically accessible 2D configuration space, reflecting on its boundaries. Reflections can be viewed as transitions to the antipode surface component glued to the original one along the boundaries. (c) Trajectories on the deformed smooth version of the resulting compact surface are shown as solid and dashed lines, which correspond to the original and antipode components, respectively.

be a matter of concern since classical dynamics constitutes an approximation for a quantum mechanical problem. The approximation is not valid near the boundaries of the classically accessible region, where the quantum uncertainty takes over. More formally, one can consider a trajectory reflected (or, equivalently, continued on the antipode replica of the accessible region) if it penetrates the near-boundary region where quantum effects become important. The classical picture of reflection becomes exact for the hard-wall potential concentrated on the boundaries as, for example, in systems similar to the Sinai billiard [38] and the Lorentz gas.

Although in a generic system the effective curvature depends on position $\boldsymbol{r}$ in configuration space, we will rationalize the qualitative picture of response in a chaotic system described above by calculating the linear and second-order classical response functions for free motion in a Riemann surface M^2 of constant negative (Gaussian) curvature. This model that allows for an exact solution has been serving as a prototype of classical chaos, as well as an example of semiclassical quantization [14,15,39].

IV. GEOMETRY AND DYNAMICS ON A RIEMANN SURFACE WITH CONSTANT CURVATURE

A. Geodesic flow

In this section we describe classical dynamics of a free particle on a compact Riemann surface M^2 of constant negative curvature (Gaussian curvature). This will be done by making use of strong dynamical symmetry. This system is one of the best studied models of chaotic dynamics. Although detailed reviews of its symmetry exist in the literature (see, e.g., Ref. [39]), we summarize the necessary results for the sake of completeness and further extension to the case of Langevin dynamics. Noisy dynamics associated with geodesic flows on surfaces with constant negative curvature is considered in detail in Ref. [32].

The Lagrangian of a free particle contains only kinetic energy: $L=mg_{ik}\dot{r}^i\dot{r}^k/2$. The corresponding unperturbed classical Hamiltonian

$$H(\boldsymbol{x},\zeta)=\frac{1}{2m}g^{ik}p_ip_k=\frac{\zeta^2}{2m} \tag{19}$$

does not depend on $\boldsymbol{r}$ and the momentum direction if expressed in terms of the absolute value of the momentum ζ. Here we introduced covariant and contravariant metric tensors g_{ik} and g^{ik}. The curvature (also referred to as the Gaussian curvature) K of configuration space M^2 can be expressed in terms of derivatives of the metric tensor:

$$K=\frac{1}{2}g^{ij}\left(\frac{\partial\Gamma^l_{ij}}{\partial r^l}-\frac{\partial\Gamma^l_{il}}{\partial r^j}+\Gamma^l_{ij}\Gamma^k_{lk}-\Gamma^k_{il}\Gamma^l_{jk}\right),$$

with the Christoffel symbols given by

$$\Gamma^k_{ij}=\frac{1}{2}g^{kl}\left(\frac{\partial g_{li}}{\partial r^j}+\frac{\partial g_{lj}}{\partial r^i}-\frac{\partial g_{ij}}{\partial r^l}\right).$$

Since unperturbed dynamics conserves energy, ζ is constant, and evolution actually occurs in the reduced phase space (energy shell) M^3. If we are not interested in a trivial case of zero energy, the distributions can be thought of as functions $\rho(\boldsymbol{x},\zeta)$, with $\boldsymbol{x}\in M^3$ and $\zeta>0$ the absolute value of the particle momentum. A compact three-dimensional smooth manifold M^3 is the subspace of the phase space that consists of points with unit length of the momentum vector. Points $\boldsymbol{x}\in M^3$ are specified by two coordinates $\boldsymbol{r}$ and the momentum direction angle θ. The dynamical symmetry for the free-particle dynamics originates from the fact that there is a smooth action of the group $G\cong \mathrm{SO}(2,1)$ in the reduced phase space of the system, consistent with the dynamics. The details are presented in Appendix B. The dynamical symmetry has a simple and clear interpretation in infinitesimal terms, i.e., action of the corresponding Lie algebra so(2,1), where the algebra generators are implemented as vector fields in M^3.

As discussed in Sec. II, the evolution in the phase space is determined by the equation $\dot{\boldsymbol{\eta}}=\hat{L}\boldsymbol{\eta}$. In this equation $\hat{L}\boldsymbol{\eta}$ is a vector field that belongs to the tangent space of the phase-space point $\boldsymbol{\eta}$. Hereafter we adopt an agreement used in differential geometry by identifying a first-order differential operator for differentiating along the vector field with the vector field itself. Due to energy conservation, the vector field $\hat{L}$ is tangent to the reduced phase space M^3. We introduce a vector field σ_1 that determines the geodesic flow and generates the translation along trajectories, so that the Liouville operator of free motion is

$$\hat{L} = \zeta\sigma_1.$$

Another natural vector field in M^3 is σ_z, which corresponds to the generator of the momentum rotation and keeps the coordinates unchanged. This operator can be represented as $\sigma_z = \partial/\partial\theta$ in terms of a derivative with respect to the particle momentum direction θ.

The operators σ_1 and σ_z can be easily expressed in terms of $\boldsymbol{r}$ and $\boldsymbol{p}$. Performing the variable transformation, we obtain

$$\sigma_1 = \frac{\partial\zeta}{\partial p_i}\frac{\partial}{\partial r_i} - \frac{\partial\zeta}{\partial r_i}\frac{\partial}{\partial p_i}, \quad \sigma_z = E_{ji}g^{jk}p_k\frac{\partial}{\partial p_i}.$$

Here E_{ij} is the asymmetric tensor, $E_{12} = -E_{21} = (\det g^{ik})^{-1/2}$, $E_{11} = E_{21} = 0$. Both operators σ_1 and σ_z obviously conserve energy: $\sigma_1\zeta = \sigma_z\zeta = 0$.

Finally, we introduce the third vector field in M^3 as $\sigma_2 = [\sigma_1, \sigma_z]$ where the commutator of vector fields is understood as the commutator of the corresponding differential operators. A simple calculation shows that in the case of constant negative curvature the vector fields σ_z, σ_1, and σ_2 form the Lie algebra so(2,1) with respect to the vector field commutator (see Appendix C for more details):

$$[\sigma_1, \sigma_2] = \sigma_z, \quad [\sigma_1, \sigma_z] = \sigma_2, \quad [\sigma_2, \sigma_z] = -\sigma_1. \tag{20}$$

The group action of SO(2,1) in the reduced phase space M^3 is obtained by integration of the algebra action.

Any compact surface of constant negative curvature may be represented as a result of factorization of the hyperbolic plane with respect to translations that constitute a finitely generated infinite discrete subgroup of SO(2,1) (see Appendix B). The entire hyperbolic plane possesses the complete SO(2,1) symmetry, which makes the infinite motion there integrable due to the presence of the integral of motion similar to the angular momentum in the case of SO(3). The factorization destroys global SO(2,1) symmetry and folds back the trajectories, which renders the dynamics strongly chaotic.

The Poisson bracket can be computed in a standard way, making use of the fact that locally it coincides with the Poisson bracket for a free particle moving in the entire hyperbolic plane H (see Appendix C). The canonical Poisson bracket may be rewritten in terms of the differential operators (vector fields) introduced above and acts on two functions $f(\boldsymbol{x}, \zeta)$ and $g(\boldsymbol{x}, \zeta)$ as

$$\{f,g\} = \frac{\partial f}{\partial\zeta}(\sigma_1 g) - (\sigma_1 f)\frac{\partial g}{\partial\zeta} + \frac{1}{\zeta}[(\sigma_2 f)(\sigma_z g) - (\sigma_z f)(\sigma_2 g)]. \tag{21}$$

The representation of the Poisson bracket as a bilinear form of the Lie algebra generators with constant coefficients is another manifestation of the dynamical symmetry of this chaotic model.

The form of the Poisson bracket as well as the commutation relations suggests that the Lyapunov exponent is equal to $\lambda = \sqrt{-K}$. This can also be clearly seen from the Jacobi equation $\ddot{y} + Ky = 0$ for the magnitude of the normal component of the deviation from a given geodesic [15]. The stable and unstable directions are given by linear combinations of σ_2 and σ_z. The displacements along the flow σ_1 are conserved. One can easily identify the algebra elements with the physical directions by considering close trajectories that start at points $(1+\sigma)\boldsymbol{\eta}$, where σ is a first-order differential operator (vector field) corresponding to a small displacement in the reduced phase space. After time interval t the trajectory is at the point $e^{\sigma_1 t}(1+\sigma)\boldsymbol{\eta}$, and, therefore, the deviation from the phase point $e^{\sigma_1 t}\boldsymbol{\eta}$ is determined by the vector field $\sigma(t) = e^{\sigma_1 t}\sigma e^{-\sigma_1 t}$. The commutation relations (20) allow us to find this Heisenberg representation of any operator decomposed over the basis elements of so(2,1). In particular, we find that

$$e^{\sigma_1 t}(\sigma_2 \pm \sigma_z)e^{-\sigma_1 t} = e^{\pm t}(\sigma_2 \pm \sigma_z), \tag{22}$$

and thus conclude that the local stable and unstable directions are given by $\sigma_2 - \sigma_z$ and $\sigma_2 + \sigma_z$, respectively. The fact that the form of these vector fields is conserved by the dynamics is also an important manifestation of the dynamical symmetry.

Dynamical symmetry also leads to the following general relation:

$$\int_{M^3} d\boldsymbol{x}\ \sigma_l f(\boldsymbol{x}) = 0 \tag{23}$$

for $l = 1$, 2, or z, which is valid for any smooth function $f(\boldsymbol{x})$, where $d\boldsymbol{x}$ in M^3 is an invariant integration measure with respect to the SO(2,1) action (see Appendix B for details). Equation (23) implies an integration by parts rule,

$$\int_{M^3} d\boldsymbol{x}\ f(\boldsymbol{x})\sigma_l g(\boldsymbol{x}) = -\int_{M^3} d\boldsymbol{x}[\sigma_l f(\boldsymbol{x})]g(\boldsymbol{x}), \tag{24}$$

which will be an important ingredient of our analytical calculations.

In conclusion we emphasize that the dynamical symmetry with respect to the action of the group $G \cong \mathrm{SO}(2,1)$ does not mean symmetry in the usual sense, i.e., that the system dynamics commutes with the group action, but rather reflects the fact that the vector field $\hat{L}$ that determines the classical dynamics is represented by an element of the corresponding Lie algebra so(2,1). This allows us to apply representation theory as described below.

B. Decomposition of the free-particle dynamics using irreducible representations

The smooth action of G in M^3 can be interpreted as follows: the space $\mathcal{H}$ of smooth functions in M^3 constitutes a representation of G, which turns out to be unitary (see Refs. [40–42] and Appendix B), and therefore can be decomposed into a direct sum of irreducible representations of G. The spectrum $\mathrm{Spec}_0(M^2) \subset \hat{G}$ of the Riemann surface is defined as a discrete subset of the space $\hat{G}$ of irreducible unitary representations of the principal series that participate in the decomposition of functions in M^3 into irreducible representations:

$$\rho(\boldsymbol{x}, \zeta) = g^{(0)}(\zeta) + \sum_{s \in \mathrm{Spec}_0(M^2)} g_s(\boldsymbol{x}, \zeta), \tag{25}$$

where $g^{(0)}(\zeta)$ is a constant in M^3 corresponding to the unit representation, and the spectrum $\mathrm{Spec}_0(M^2)$ consists of

imaginary numbers s that characterize representations of the principal series. The relevance of other (complementary and discrete) series is discussed after their review in Appendixes B and D. The evolution in the space of distributions is decomposed into a set of uncoupled evolutions in the relevant irreducible representations. The component dynamics is determined by the reduced Liouville operators

$$\frac{\partial g_s(\boldsymbol{x},\zeta;t)}{\partial t} = -\zeta \hat{L}(s) g_s(\boldsymbol{x},\zeta;t), \tag{26}$$

where $\hat{L}(s)$ corresponds to an irreducible representation labeled by s. The distribution components can be further decomposed as

$$g_s(\boldsymbol{x},\zeta) = \sum_{k=-\infty}^{\infty} \rho_{s,k}(\zeta)\psi_k(\boldsymbol{x};s), \tag{27}$$

using the eigenstates $\psi_k(\boldsymbol{x};s)$ of the angular momentum operator σ_z. These satisfy the following properties:

$$\sigma_z \psi_k(\boldsymbol{x};s) = ik\psi_k(\boldsymbol{x};s),$$

$$\sigma_\pm \psi_k(\boldsymbol{x};s) = \left(\pm k + \frac{1}{2} - s\right)\psi_{k\pm 1}(\boldsymbol{x};s), \tag{28}$$

where we introduced the raising and lowering operators $\sigma_\pm = \sigma_1 \pm i\sigma_2$ which are anti-Hermitian conjugated, i.e., $\sigma_+^\dagger = -\sigma_-$.

According to the description of unitary representations of G, reviewed in detail in Appendix D (see also Refs. [41,42]), the eigenstates $\psi_k(\boldsymbol{x};s)$ can be represented by the functions on the circle $\Psi_k(u)$ for any given $s \in \mathrm{Spec}(M^2)$. In the case of imaginary s (principal series), when $\Psi_m(u)$ constitutes an orthogonal normalized set with the natural scalar product, this leads to normalized functions $\psi_k(\boldsymbol{x};s)$. Identification of the functions $\psi_k(\boldsymbol{x})$ with $\Psi_k(u)$ establishes an isomorphism between two irreducible representations, the first being $\mathcal{H}_s$, which participates in the decomposition of Eq. (B4), the second being its standard representation in function in a circle described in Appendix D. According to the Shur lemma (see, e.g., [40]) the identification (isomorphism) is determined up to a factor. Its absolute value can be fixed by requiring that the function $\psi_0(\boldsymbol{x};s)$ identified with $\Psi_0(u)=1$ is normalized. To fix its phase also, we note that $\psi_0(\boldsymbol{x};s)$ does not depend on θ and turns out to be an eigenfunction of the Laplacian in M^2 as described by Eq. (D5). Since the Laplacian is a real operator, the eigenfunction $\psi_0(\boldsymbol{x};s)$ can be chosen to be real. Hereafter, we implement an agreement that $\psi_0(\boldsymbol{x};s)$ identified with $\Psi_0(u)=1$ is real. This determines the functions up to a sign, the latter being of no importance: $\Psi_k(u)=e^{iku}$.

The form of σ_1 in the angular representation is fixed up to a phase [41]:

$$\hat{L}(s) = \sigma_1 = \sin u \frac{d}{du} + \frac{1-2s}{2}\cos u. \tag{29}$$

Thus, the original dynamics of a distribution $g_s(\boldsymbol{x};s)$ in Eq. (27) is mapped onto an effective classical dynamics of a distribution $\mathcal{G}(u)=\Sigma_{k=-\infty}^{\infty}\rho_{s,k}(\zeta)\Psi_k(u;s)$ defined on a circle with the Liouville operator (29). The resulting effective problem is one dimensional and can be solved exactly.

The term that describe the interaction with the driving field can be also decomposed in irreducible representations. The coupling (polarization) f is represented by a function of the particle position only (i.e., a function in M^2). It can be equivalently interpreted as a function in M^3 independent of θ, hence $\sigma_z f=0$. Thus, f can be expanded as

$$f = \sum_{s\in \mathrm{Spec}_0(M^2)} B_s \psi_0(\boldsymbol{x};s). \tag{30}$$

The sum in Eq. (30) runs over the spectrum of the compact surface corresponding to the principal series representations characterized by imaginary s (see Appendix D). We recall that the functions $\psi_0(\boldsymbol{x};s)$, being actually functions of the particle position only, are the eigenfunctions of the Laplacian on the compact Riemann surface of constant negative curvature. We should note that these eigenfunctions are tangible and intuitively simple objects, although the diagonalization Laplacian might be a complex problem. Typically the dipole distribution f is a slow function of coordinates, and therefore only a few terms provide substantial contributions to the expansion of Eq. (30). Combined with the previous results, the expansion leads to closed analytical expressions for the response functions of the original problem.

C. Effective dynamics on the circle

We have identified the dynamical symmetry that allows the original chaotic dynamics on M^2 to be mapped onto a tractable dynamical problem on the circle. In this subsection we consider the dynamics that corresponds to a principal series representation labeled by s with $\mathrm{Im}\, s>0$. In the following calculations of the response functions, we will need the expansion of $e^{-\hat{L}t}\psi_0(\boldsymbol{x};s)$ in the basis vectors $\psi_k(\boldsymbol{x};s)$,

$$e^{-\hat{L}t}\psi_0(\boldsymbol{x};s) = \sum_{k=-\infty}^{+\infty} A_k(t;s)\psi_k(\boldsymbol{x};s). \tag{31}$$

In particular, the linear response is expressed in terms of the coefficient A_0. The coefficients A_k are actually matrix elements of the evolution operator between the angular harmonics and have been calculated earlier [22,39]. The result immediately follows from the description of irreducible representations using a construction of an induced representation (see, e.g., Ref. [41]). The derivation presented below allows us to regularize the original classical response problem by introducing weak noise and treat the resulting stochastic model using the Fokker-Planck formalism in Ref. [32].

The coefficients $A_k(t;s)$ can be calculated by implementing the representation on the circle introduced above. The function $g(t,u)=e^{-\hat{L}(s)t}\Psi_0(u)$, where $\Psi_0(u)\equiv 1$, can be found by solving the dynamical equation $\partial_t g(t,u)+\hat{L}(s)g(t,u)=0$ supplemented with an initial condition $g(0,u)=1$. For the principal series representation labeled by s, the equation adopts the following form:

$$\partial_t g(t,u) + \left(\sin u \frac{\partial}{\partial u} + \frac{1-2s}{2}\cos u\right) g(t,u) = 0. \quad (32)$$

The method of characteristics yields:

$$e^{-\hat{L}(s)t}\Psi_0(u) = e^{st-t/2}\left|\cos\frac{u}{2}\right|^{2s-1}\left(1+e^{-2t}\tan^2\frac{u}{2}\right)^{s-1/2}$$
$$= (\cosh t + \sinh t \cos u)^{s-1/2}. \quad (33)$$

At long times $t>0$ the solution is concentrated near the stable stationary point $u=\pi$. This reflects the collapse of the reduced phase-space distribution function along the stable direction. Indeed, the width of the region where $e^{-\hat{L}(s)t}\Psi_0(u)$ is not exponentially small vanishes as $\propto e^{-t}$, according to the value $\sqrt{-K}=1$ of the Lyapunov exponent for the chaotic dynamics on M^2 with the constant Gaussian curvature $K=-1$.

The expansion coefficients in Eq. (31) are given by

$$A_k(\zeta t;s) = \int \frac{du}{2\pi}\Psi_k^*(u)e^{-\zeta\hat{L}(s)t}\Psi_0(u). \quad (34)$$

The integral can be reduced to a standard integral representation of the Gauss hypergeometric function ${}_2F_1(a,b,c,z)$ defined as a series,

$${}_2F_1(a,b,c,z) = \sum_{n=0}^{\infty}\frac{\Gamma(a+n)\Gamma(b+n)\Gamma(c)}{\Gamma(a)\Gamma(b)\Gamma(c+n)n!}z^n, \quad (35)$$

with $\Gamma(z)$ being the gamma function [43]. If $k\geq 0$, the exact expression for A_k reads

$$A_k(t;s) = (-1)^k\frac{\Gamma\left(k+\frac{1}{2}-s\right)}{k!\,\Gamma\left(\frac{1}{2}-s\right)}\left(\tanh\frac{t}{2}\right)^k$$
$$\times {}_2F_1\left(\frac{1}{2}+s,\frac{1}{2}-s,k+1,-\sinh^2\frac{t}{2}\right). \quad (36)$$

Various representations of these coefficients using other special functions have been derived in the context of two-point correlations [22,39].

Since the solution g of Eq. (32) is even, $g(t,-u)=g(t,u)$, the coefficients A_k are symmetric, $A_{-k}=A_k$. The time-reversal property

$$g(-t,u) = g(t,u+\pi), \quad (37)$$

which follows directly from Eq. (32), immediately implies $A_k(-t)=(-1)^k A_k(t)$. We can represent $A_k(t;s)$ in an alternative form suitable for studying its long-time behavior [43]:

$$A_k(t;s) = \frac{2(-1)^k(1-e^{-2t})^k\Gamma\left(k+\frac{1}{2}-s\right)}{\sqrt{\pi}\Gamma\left(\frac{1}{2}-s\right)}e^{-t/2}$$
$$\times \mathrm{Re}\left[\frac{\Gamma(s)e^{st}}{\Gamma\left(k+\frac{1}{2}+s\right)}\,{}_2F_1\left(k+\frac{1}{2}-s,k+\frac{1}{2},1-s,e^{-2t}\right)\right]. \quad (38)$$

Its expansion in e^{-2t} using Eq. (35) corresponds to the spectral decomposition of the regularized evolution operator for the irreducible representation labeled by s. The properly interpreted eigenvalues of the Liouville operator are known as Ruelle-Pollicott resonances for chaotic systems. They can be obtained by considering the dynamics with weak Langevin noise, which amounts to adding an infinitesimal second-order differential diffusion operator to the classical Liouville operator, $\hat{\mathcal{L}}=-\kappa\hat{D}+\hat{L}$, where the diffusion coefficient (tensor) κ is given by the noise intensity. The resulting Fokker-Planck operator $\hat{\mathcal{L}}$ has a well-defined spectrum in the space of smooth physical functions [16]. The Ruelle-Pollicott resonances are more often treated as mathematical objects in terms of generalized eigenfunctions in a properly chosen rigged Hilbert space (see, e.g., Ref. [22]). Our physical approach to spectral decomposition of linear and nonlinear response functions for a free particle moving on a surface of constant negative curvature is presented in the following paper [32].

We will be interested in the long-time behavior of the response functions, and expect that the asymptotics

$$A_k(t;s) \approx \frac{2(-1)^k\Gamma\left(k+\frac{1}{2}-s\right)}{\sqrt{\pi}\Gamma\left(\frac{1}{2}-s\right)}e^{-t/2}\,\mathrm{Re}\left(\frac{\Gamma(s)e^{st}}{\Gamma\left(k+\frac{1}{2}+s\right)}\right) \quad (39)$$

at $t\to\infty$ are relevant. However, we will see that, since the approximation breaks down for higher harmonics $k\gtrsim e^t$ and does not vanish at $k\to\infty$, it cannot be immediately utilized for nonlinear response calculations where the result is given by an infinite series over k. In the region $t\gtrsim 1$ and $1\ll k \ll e^{2t}$ one can use an approximation for $A_k(t)$ in terms of the MacDonald function (modified Bessel function of the second kind):

$$A_k(t;s) \approx \frac{2(-1)^k}{\sqrt{\pi}\Gamma\left(\frac{1}{2}-s\right)}e^{-t/2}k^{-s}K_s(2ke^{-t}). \quad (40)$$

V. CALCULATION OF RESPONSE FUNCTIONS

In this section we substantiate the semiquantitative picture of response presented in Sec. III for a particular model of

free motion on a compact surface with constant negative curvature. Heretofore we have not made any assumptions about the shape of the initial distribution ρ_0 in the general expressions for response functions. In the case of free motion, the equilibrium phase-space density ρ_0 depends on the momentum absolute value only. The fluctuation-dissipation theorem relates the linear response function to the correlation function in a system at thermal equilibrium. To reduce bulky calculations, in both linear and second-order response functions, we employ an analog of the FDT [23]. Thus Eqs. (10) and (11) can be recast as follows:

$$S^{(1)}(t_1) = \partial_{t_1} \int d\boldsymbol{\eta}\, f(\boldsymbol{\eta}) e^{-\hat{L}t_1} f(\boldsymbol{\eta}) \frac{\partial \rho_0}{\partial \zeta}, \tag{41}$$

$$S^{(2)}(t_1,t_2) = \partial_{t_1} \int d\boldsymbol{\eta}\, f(\boldsymbol{\eta}) e^{-\hat{L}t_2} \left\{ f(\boldsymbol{\eta}), e^{-\hat{L}t_1} f(\boldsymbol{\eta}) \frac{\partial \rho_0}{\partial \zeta} \right\}. \tag{42}$$

The general expressions given by Eqs. (41) and (42) apply to any equilibrium distribution, including the canonical $\rho_0 \propto e^{-\beta E}$, microcanonical $\rho_0 \propto \delta(E-E_0)$, and cumulative microcanonical $\partial_E \rho_0 \propto \delta(E-E_0)$ distributions. To obtain the final expressions in the most transparent form we will use the cumulative microcanonical distribution with the cutoff energy $E_0=1/2$.

We are able to approach an apparently intractable problem of calculating the response in a chaotic system because of the strong dynamical symmetry. The preliminary steps of our calculation have been described in the preceding section. Dynamical symmetry leads to decomposition of the original dynamical problem into a set of uncoupled evolutions in irreducible representations of the dynamical symmetry group SO(2,1). The dipole moment f is expanded over momentum-independent basis functions $\psi_0(\boldsymbol{x};s)$ according to Eq. (30), where s labels relevant irreducible representations. The relevant matrix elements $A_k(t;s)$ of the evolution (Perron-Frobenius) operator are given by Eq. (36). The coefficients $A_k(t;s)$ constitute the dynamical part in the calculation of the response functions. The geometrical part of the calculation is represented by the integrals over the reduced phase space, hereafter referred to as (geometrical) matrix elements. The geometrical part turns out to be trivial in the linear response case whereas the calculations for the second-order response are more involved.

In this section for the sake of simplicity the calculations are performed in the case when the dipole moment f has a single component (a single eigenfunction of the Laplace operator), $f=\psi_0(\boldsymbol{x};s)$, in the expansion over irreducible representations (30). Some details for the case of two components, $f=B_{s_1}\psi_0(\boldsymbol{x};s_1)+B_{s_2}\psi_0(\boldsymbol{x};s_2)$ (superposition of two Laplacian eigenmodes), are given in Appendix E. Numerical results for the second-order response function in this simplest case that involves different resonances are presented in Sec. VI.

A. Linear response

Since the basis functions $\psi_k(\boldsymbol{x};s)$ with different k are mutually orthogonal, the linear response function is determined by the dynamical part alone and can be represented in the form

$$S^{(1)}(t) = \frac{\partial}{\partial t} \int_0^\infty d\zeta\, A_0(\zeta t;s) \frac{\partial \rho_0}{\partial \zeta}, \tag{43}$$

with

$$A_0(t;s) = \frac{2}{\sqrt{\pi}} e^{-t/2} \mathrm{Re}\left[\frac{\Gamma(-s) e^{-st}}{\Gamma\left(\frac{1}{2}-s\right)} {}_2F_1\left(\frac{1}{2}+s, \frac{1}{2}, 1+s, e^{-2t}\right) \right] \tag{44}$$

according to Eq. (38). For large t the linear response function shows oscillatory decay as $e^{-(1/2\pm s)t}$. The expansion in powers of e^{-2t} can be interpreted as the expansion over Ruelle-Pollicott resonances [22]. The resonances can be found as the eigenvalues of the regularized Liouville operator [32]. Only even resonances $\omega_{2k}=2k+1/2\pm s$ contribute to the response function. The expansion is a convergent series over e^{-2t_1} if $e^{-2t_1}<1$, i.e., $t_1>0$.

In a general case the coupling $f(\boldsymbol{x})$ can be decomposed over irreducible representations labeled by s [see Eq. (30)], and the linear response function becomes a linear combination of contributions (43) with the coefficients B_s^2. Due to orthogonality of the basis functions, there is no coupling between different representations.

B. Second-order response: matrix elements

The second-order response function for a free particle on a Riemann surface with constant negative curvature is obtained by substituting the specific expression for the Poisson bracket [Eq. (21)] into the generic expression given by Eq. (42). We further simplify the calculation by making use of the evolution operator unitarity $(e^{-\hat{L}t_2})^\dagger = e^{\hat{L}t_2}$ with respect to the natural scalar product defined by Eq. (D2). Performing the integration over ζ by parts and making use of $\partial\rho_0/\partial\zeta|_{\zeta=0,\infty}=0$ results in

$$\begin{aligned} S^{(2)}(t_1,t_2) = \frac{\partial}{\partial t_1} \int d\boldsymbol{x}\, d\zeta [& \zeta t_2 (\sigma_1 e^{\sigma_1 \zeta t_2} f)^* (\sigma_1 f)(e^{-\sigma_1 \zeta t_1} f) \\ & + (e^{\sigma_1 \zeta t_2} f)^* (\sigma_1 f)(e^{-\sigma_1 \zeta t_1} f) + (e^{\sigma_1 \zeta t_2} f)^* (\sigma_2 f) \\ & \times (\sigma_z e^{-\sigma_1 \zeta t_1} f)] \frac{\partial \rho_0}{\partial \zeta}. \end{aligned} \tag{45}$$

The transformation to Eq. (45) is an important step toward expressing the result in terms of the quantities calculated in the previous sections. This allows us to avoid propagating the vector fields σ_2 and σ_z, and instead to deal only with the action of the evolution operators $e^{\hat{L}t_2}$ and $e^{-\hat{L}t_1}$ on the dipole distribution f. The latter is decomposed according to Eq. (30) into zero harmonics $\psi_0(\boldsymbol{x};s)$ of irreducible representations labeled by s, i.e., the Laplacian eigenmodes. Then we use the expansion (31) to express $e^{-\hat{L}t}\psi_0(\boldsymbol{x};s)$ in terms of the angular harmonics $\psi_k(\boldsymbol{x};s)$ which constitutes a basis set in the representation.

Now we approach the most challenging part of the calculation represented by the integration over the reduced phase

space. Generally, according to the decomposition of f, the integration may involve functions from different irreducible representations. In this section we consider the simplest case $f=\psi_0(\boldsymbol{x};s)$ of the dipole function represented by a single eigenmode of the Laplacian. A more complicated case of two representations is treated in Appendix E.

The second-order response function calculation involves the integrals of $\psi_n^*(\boldsymbol{x};s)[\sigma_{1,2}\psi_0(\boldsymbol{x};s)]\psi_m(\boldsymbol{x};s)$, referred to as matrix elements, that are substantially less trivial than their counterparts in the linear response function. In the latter case the integrals of the double product of $\psi_n(\boldsymbol{x};s)$ can be calculated based on orthogonality and normalization of the functions. The challenge arises from the fact that integrals of triple products over the reduced phase space do not have a natural representation on the circle. Nevertheless, we will show that this geometrical part of the second-order response can be worked out using relatively simple tools, and can be expressed in terms of a few quantities related to the Laplacian eigenmodes.

The integration in the reduced phase space $M^3 \ni \boldsymbol{x}$ is performed over the particle coordinates $\boldsymbol{r}\in M^2$ and the locally defined angle θ that represents the 2D momentum direction. A local (for fixed $\boldsymbol{r}$) dependence of $\psi_n(\boldsymbol{x};s)$ on θ is given by $\psi_n(\boldsymbol{x};s)\propto e^{in\theta}$ due to the definition $\partial_\theta\psi_n(\boldsymbol{x};s)=in\psi_n(\boldsymbol{x};s)$ of the basis functions. The operators σ_1 and σ_2 applied to $\psi_0(\boldsymbol{x};s)$ in the middle of the integrand are expressed via the ladder operators $\sigma_\pm$. Therefore, the integration over θ in Eq. (45) results in zero unless the integrand is locally independent of θ, i.e.,

$$\int_{M^3} d\boldsymbol{x}[\psi_n(\boldsymbol{x};s)]^*[\sigma_\pm\psi_0(\boldsymbol{x};s)]\psi_m(\boldsymbol{x};s)\propto\delta_{n,m\pm1}. \quad (46)$$

We now introduce matrix elements a_k and b_k as

$$a_k=\int_{M^3} d\boldsymbol{x}\ \psi_k^*(\boldsymbol{x};s)\psi_0(\boldsymbol{x};s)\psi_k(\boldsymbol{x};s), \quad (47)$$

$$b_k=2\int_{M^3} d\boldsymbol{x}\ \psi_k^*(\boldsymbol{x};s)[\sigma_+\psi_0(\boldsymbol{x};s)]\psi_{k-1}(\boldsymbol{x};s). \quad (48)$$

As established in Sec. IV, the differential operators $\sigma_\pm$ behave as simple derivatives in the integration by parts. Using the properties (28) of σ operators, we derive the following implicit recurrence relations:

$$\begin{aligned} b_{k+1}&=2\int d\boldsymbol{x}\ \psi_{k+1}^*(\sigma_+\psi_0)\psi_k\\ &=-2\int d\boldsymbol{x}(\sigma_-\psi_{k+1})^*\psi_0\psi_k-2\int dx\ \psi_{k+1}^*\psi_0\sigma_+\psi_k\\ &=(2k+1-2s)(a_k-a_{k+1}) \end{aligned} \quad (49)$$

and

$$\begin{aligned} b_{k+1}&=2\int d\boldsymbol{x}\ \psi_{k+1}^*(\sigma_+\psi_0)\psi_k\\ &=\frac{4}{2k+1+2s}\int d\boldsymbol{x}(\sigma_+\psi_k)^*(\sigma_+\psi_0)\psi_k\\ &=-\frac{4}{2k+1+2s}\int d\boldsymbol{x}\ \psi_k^*((\sigma_-\sigma_+\psi_0)\psi_k+(\sigma_+\psi_0)\sigma_-\psi_k)\\ &=\frac{1-4s^2}{2k+1+2s}a_k+\frac{2k-1+2s}{2k+1+2s}b_k. \end{aligned} \quad (50)$$

The recurrence relations between the matrix elements can be recast in the explicit form:

$$\begin{aligned} a_{k+1}&=\frac{4k(k+1)}{(2k+1)^2-4s^2}a_k-\frac{2k-1+2s}{(2k+1)^2-4s^2}b_k,\\ b_{k+1}&=\frac{1-4s^2}{2k+1+2s}a_k+\frac{2k-1+2s}{2k+1+2s}b_k. \end{aligned} \quad (51)$$

The matrix elements b_k can be excluded, which results in a relation between a_{k-1}, a_k, and a_{k+1}:

$$a_{k+1}=\frac{8k^2+1-4s^2}{(2k+1)^2-4s^2}a_k-\frac{(2k-1)^2-4s^2}{(2k+1)^2-4s^2}a_{k-1}. \quad (52)$$

As mentioned earlier, ψ_0 can be chosen real, which leads to the relations $a_1=a_{-1}=a_0/2$ (see Appendix E for the details). Thus, all matrix elements a_k can be expressed in terms of a single real number a_0.

Putting all contributions to the second-order response function together, we can express it in the following form:

$$\begin{aligned} S^{(2)}=\int d\zeta\frac{\partial\rho_0}{\partial E}\sum_{n=0}^{\infty}(-1)^n(a_n-a_{n+1})\left(n+\frac{1}{2}+s\right)\\ \times\frac{\partial}{\partial t_1}\left(\frac{\partial}{\partial t_2}\{t_2[A_{n+1}(\zeta t_1)A_n^*(\zeta t_2)-A_n^*(\zeta t_1)A_{n+1}(\zeta t_2)]\}\right.\\ \left.-[(n+1)A_{n+1}(\zeta t_1)A_n^*(\zeta t_2)+nA_n^*(\zeta t_1)A_{n+1}(\zeta t_2)]\right). \end{aligned} \quad (53)$$

Here we used the short notation $A_n(t)$ for $A_n(t;s)$ and the fact that the product $(2n+1-2s)A_{n+1}^*(t_2;s)A_n(t_1;s)$ is real. We used the symmetries $A_{-n}(t)=A_n(t)$ and $a_{-n}=a_n$ discussed in Sec. IV C and Appendix E to restrict the series summation to $n\geq 0$.

We note that the coefficients $A_n(-t_2;s)$ at negative time $-t_2<0$, which enter the expansion for the backward evolution of $\psi_0(\boldsymbol{x};s)$, were replaced by $(-1)^{-n}A_n(t_2;s)$ due to the time-reversal symmetry.

The result for the second-order response function (53) is written in the form of an ordinary series of terms whose expressions are either completely known analytically [see Eq. (36)] or recurrently expressed via a single number a_0 that characterizes the function $\psi_0(\boldsymbol{x};s)$. The functions ψ_0 do not depend on the angle θ, i.e., $\psi_0(\boldsymbol{x})=\phi(\boldsymbol{r};\mu)$, where, according to Eq. (D6), $\phi(\boldsymbol{r};\mu)$ is an eigenmode of the Laplace operator with the eigenvalue μ on the Riemann surface. Therefore,

Eqs. (B3) and (D6) allow the only undetermined parameters s and a_0 in Eq. (53) to be expressed in terms of the relevant eigenmode $\phi(\boldsymbol{r};\mu)$ of the Laplacian:

$$a_0 = \int_{M^2} d\boldsymbol{r}[\phi(\boldsymbol{r};\mu)]^3, \quad s = \frac{i\sqrt{-4\mu-1}}{2}. \tag{54}$$

Finding the eigenmodes of the Laplacian analytically is a complex problem. Fortunately its explicit solution is not necessary for our purposes. It is known that for a given constant negative curvature $K<0$ there is a family of nonequivalent Riemann surfaces of genus g that can be parametrized by a space $\mathcal{M}_g$ (known as a moduli space) [39,41] with the dimension $\dim \mathcal{M}_g = 4g-2$. In particular, a_0 and s can be viewed as some nontrivial functions on the moduli space $\mathcal{M}_g$ whose computation is a complex problem. We can treat a_0 and s as free parameters that characterize some Riemann surface of constant negative curvature.

In a more general case, when the dipole f is represented by a finite superposition of N_f Laplacian eigenmodes, the second-order response can be expressed in terms of a larger set of parameters s_j and $a_0^{s_i s_j s_k}$, with $i,j,k=1,\ldots,N_f$ as described in Appendix E. We can apply the same argument to treat them as free parameters for a Riemann surface of a high enough genus g.

C. Second-order response: Summation of the series

We have expressed the second-order response in terms of an ordinary converging series for the cases of a single Laplacian mode $N_f=1$ [Eq. (53)] and two modes $N_f=2$ [Eq. (E7)], respectively, in the expansion of the dipole (30). A general expression for a finite number N_f of modes has a similar structure. Each term of the series is known analytically in the form that involves special functions and solutions of recurrence relations. Or goals are to derive the long-time asymptotics of the second-order response $S^{(2)}$, and develop a computationally efficient procedure for $S^{(2)}(t_1,t_2)$ at finite times.

We start with the asymptotic behavior of the second-order response function for large t_1 and t_2. Naively, one would plug the long-time asymptotic of $A_n(t;s)$ from Eq. (39) into Eq. (53). However, this asymptotic of $A_n(t;s)$ is valid only for fixed n, if $ne^{-t} \ll 1$. This can be confirmed by comparing the consecutive terms in the expansion of the hypergeometric function in Eq. (36) in powers of e^{-t}. Moreover, although $A_n(t;s)$ represent the Fourier expansion coefficients of a smooth function (33), their asymptotic (39) does seem to vanish as $n\to\infty$. Counting the powers of n in the second part of the summand in Eq. (53) estimated using these asymptotic expressions reveals that the resulting series fails to converge.

Indeed, the series (53) can be represented in the form

$$S^{(2)}(t_1,t_2) = \sum_{n=0}^{\infty} (-1)^n F(n;t_1,t_2), \tag{55}$$

where the dependence of $F(n;t_1,t_2)$ on n is slow for $n\gg 1$. We may find the long-time behavior of the terms as

$$F(n;t_1,t_2) = \sum_{k,l=0}^{\infty} F_{kl}(n;t_1,t_2)e^{-2kt_1-2lt_2}. \tag{56}$$

The double expansion originates from the products $A_m^*(t_1;s)A_n(t_2;s)$ where $A_n(t;s)$ is expanded in powers of e^{-2t}. The first term in the expansion of $A_n(t;s)$ [see Eq. (39)] turns out to be independent of n in the limit of large n, apart from irrelevant slow quasioscillations proportional to n^s that cannot affect the series convergence. A naive long-time asymptotic of the series is given by $\Sigma_n(-1)^n F_{00}(n;t_1,t_2)$, where the nth term is estimated as

$$F_{00}(n;t_1,t_2) = n^2(a_n - a_{n+1})e^{-t_1+t_2/2}\mathrm{Re}[C_n(s)e^{st_1}]\mathrm{Re}[D_n(s)e^{st_2}]. \tag{57}$$

Here the quasioscillatory dependence of a_n, $C_n(s)$, and $D_n(s)$ on $n\gg 1$ does not affect the convergence. Taking into account the asymptotic form of a_n [see Eq. (F1)], we conclude that the series is obviously divergent as $\Sigma_n(-1)^n F_{00}(n;t_1,t_2)\sim\Sigma_n(-1)^n\sqrt{n}$. In what follows we show how to overcome the apparent divergence and calculate the asymptotic of the second-order response function analytically.

The series in Eq. (55) that represents the response function must converge for fixed values of t_1 and t_2. Indeed, the terms $F(n;t_1,t_2)\propto\exp[-2n(e^{-t_1}+e^{-t_2})]$ vanish exponentially, although only for extremely large $n\gg e^{t_1},e^{t_2}\gg 1$. This decay rate is determined by the fact that $g(t,u)\equiv e^{-\hat{L}t}\Psi_0(u)$ is smooth on scales that do not exceed the smallest fettuccine dimension e^{-t} [see Eq. (33)]. The ultimate convergence allows us to safely regroup the terms of the series:

$$\sum_{n=0}^{\infty}(-1)^n F(n) = \frac{1}{2}F(0) + \frac{1}{2}\sum_{k=0}^{\infty}[F(2k) - 2F(2k+1) + F(2k+2)], \tag{58}$$

where $F(n)$ stands for $F(n;t_1,t_2)$. After the terms are regrouped, the initial naive approach based on approximating $F(n;t_1,t_2)$ by its long-time asymptotic $F_{00}(n;t_1,t_2)$ results in a converging series, since the linear combination in the summand represents the discrete counterpart of the second derivative $d^2F_{00}(n)/dn^2$ which decays proportionally to $n^{-3/2}$. According to Eq. (57) there are four types of time dependence in the resulting series. Therefore, the long-time asymptotic of the response function $S^{(2)}(t_1,t_2)$ is represented by a superposition of four components $e^{-(t_1+t_2)/2\pm s(t_1\pm t_2)}$ with the coefficients in the form of convergent series.

The coefficients $F_{kl}(n;t_1,t_2)$ at higher orders in the expansion (56) grow faster with increasing n than $F_{00}(n;t_1,t_2)$, as $F_{kl}(n;t_1,t_2)\sim n^{2(n+k)}F_{00}(n;t_1,t_2)$. The regrouping approach of Eq. (58) can be generalized to eliminate the apparent divergences for higher-order terms in Eq. (56), and obtain the higher-order terms in the asymptotic expansion of the second-order response in powers of e^{-2t_1} and e^{-2t_2}. Instead of that we suggest an alternative procedure that allows us to (i) demonstrate the existence of a long-time asymptotic expansion of $S^{(2)}$ in powers of e^{-2t_1} and e^{-2t_2}, (ii) derive relatively simple expressions for the expansion coefficients in any order, and (iii) develop an efficient numerical scheme for computation of the response at finite times.

We start with deriving an asymptotic expansion. To that end, provided $t_1, t_2 \gg 1$, we introduce an intermediate $N \gg 1$, so that for $n > N$ the terms $F(n;t_1,t_2)$ are represented by smooth functions of n. We further partition the sum S of the series into the finite sum $S_N = \Sigma_{n \le N}(-1)^n F(n)$ and the remainder $R_N = \Sigma_{n>N}(-1)^n F(n)$, followed by evaluating the remainder. Implementing the definition [43] of the Euler polynomials $E_n(y)$, we derive the following identity, based on the Taylor expansion of $(1+e^{-x})^{-1}$ in $x = d/dz$:

$$F(z+1) - F(z) = \sum_{n=0}^{\infty} \frac{E_n(1)}{2n!} \frac{d^n}{dz^n}[F(z+1) - F(z-1)],$$

which is used to calculate the sum of consecutive terms pairwise, so that the remainder $R_N = \Sigma_{n>N}(-1)^n F(n)$ of the almost alternating series becomes related to the first term $F(N)$ that is not included in R_N, and its derivatives:

$$\begin{aligned} R_N &= \frac{(-1)^{N+1}}{2} \sum_{m=0}^{\infty} \frac{E_m(1)}{m!} F^{(m)}(N) \\ &= \frac{(-1)^{N+1}}{2} \sum_{m=0}^{n} \frac{E_m(1)}{m!} F^{(m)}(N) + O(F^{(n+1)}(N)) \\ &= (-1)^{N+1} \left(\frac{1}{2} F(N) + \frac{1}{4} F'(N) + \cdots \right). \end{aligned} \tag{59}$$

We further introduce the following "improved" partial sums:

$$P_N^{(M)} = S_N + \frac{(-1)^{N+1}}{2} \sum_{m=0}^{M} \frac{E_m(1)}{m!} F^{(m)}(N), \tag{60}$$

so that $S^{(2)} = P_N^{(M)} + O(F^{(M+1)}(N))$. Due to the smoothness of $F(n)$ the deviation of $S^{(2)}$ from its improved approximation $P_N^{(M)}$ may be estimated as $\sim F(N)/N^{(M+1)}$. Since $P_N^{(M)}$ are determined by $F(z)$ for $z < N$, a choice of $N \ll e^{t_1}, e^{t_2}$ allows the expansion of Eq. (56) to be used, which leads to an expansion of $P_N^{(M)}$,

$$P_N^{(M)}(t_1,t_2) = \sum_{m_1 m_2} P_{N,m_1 m_2}^{(M)}(t_1,t_2) e^{-2(m_1 t_1 + m_2 t_2)}, \tag{61}$$

in powers of e^{-2t_1} and e^{-2t_2} with

$$\begin{aligned} P_{N,m_1 m_2}^{(M)} &= \sum_{k=0}^{N} (-1)^k F_{m_1 m_2}(k;t_1,t_2) \\ &\quad + \frac{(-1)^{N+1}}{2} \sum_{m=0}^{M} \frac{E_m(1)}{m!} \partial_N^m F_{m_1 m_2}(N;t_1,t_2). \end{aligned} \tag{62}$$

The reason for introducing the improved partial sums $P_N^{(M)}$ is that the expressions for the expansion coefficients $P_{N,m_1 m_2}^{(M)}$ have finite limits at $N \to \infty$ provided $M > m_1 + m_2$. Stated differently, the second term in Eq. (62) can be viewed as a set of counterterms that eliminate the divergence in the first term. In the limit $N \to \infty$ Eq. (61) leads to the expansion

$$S^{(2)}(t_1,t_2) = \sum_{m_1 m_2} S_{m_1 m_2}^{(2)}(t_1,t_2) e^{-2(m_1 t_1 + m_2 t_2)} \tag{63}$$

with

$$S_{m_1 m_2}^{(2)}(t_1,t_2) = \lim_{N \to \infty} P_{N,m_1 m_2}^{(m_1+m_2)}(t_1,t_2). \tag{64}$$

The expansion in Eq. (63) is an asymptotic rather than converging series. It can be viewed as a double expansion of the second-order response function $S^{(2)}(t_1,t_2)$ in Ruelle-Pollicott resonances which originates from the uncoupled evolutions of the chaotic system during time intervals t_1 and t_2. This will be demonstrated explicitly [32] by analyzing the noiseless limit of the corresponding Langevin dynamics.

At this point we should note that our derivation of the asymptotic expansion has been somewhat frivolous. First of all, since the terms $F(n;t_1,t_2)$ of our original series involve the coefficients a_n, we do not actually know an analytical function $F(z;t_1,t_2)$ that represents the summand, only its values for positive integer $z=n$ are available. In particular the derivatives $\partial_N^n F_{m_1 m_2}(N)$ in Eq. (62) have not been defined yet. Second, in obtaining the asymptotic expansion we were not controlling the neglected terms. This is especially dangerous in our case since we derive the complete asymptotic, which involves computing the terms that are exponentially small compared to more senior terms in the expansion. We need to make sure that the terms that are neglected in computing a certain expansion coefficient are small also compared to the higher terms that are kept in the asymptotic expansion.

A sketch of the appropriate derivation is presented in Appendix F. In particular, we demonstrate that the coefficients a_n that enter the expressions for $F(n;t_1,t_2)$ can be represented by some analytical function $a(z)$, and therefore the terms $F(n;t_1,t_2)$ of the original series are represented by some analytical function $F(z;t_1,t_2)$. We will further demonstrate how to compute derivatives $F^{(m)}(N)$ without explicit knowledge of the function $F(z)$. We also show how a proper choice of N and n in $P_N^{(M)}$ allows us to control terms neglected in the asymptotic expansion.

In the remainder of this section we will implement the summation procedure in the form of an efficient numerical scheme for computing the second-order response $S^{(2)}(t_1,t_2)$ at arbitrary times. We reiterate that all terms in the series for $S^{(2)}$ are known in their analytical form (via recurrence relations) apart from a few parameters determined by the geometry of the surface, as discussed at the end of the previous section and in Appendix E.

In the simplest case $N_f = 1$ the single parameter is given by Eq. (54). The series for $S^{(2)}$ is absolutely convergent, which becomes remarkable only at $n \gtrsim e^{t_1}$ or $n \gtrsim e^{t_2}$, and therefore a straightforward computation involves a number of terms with relatively complex structure that is exponentially growing with time. At given times t_1 and t_2, the terms $F(n;t_1,t_2)$ of the series constitute a sequence of numbers. Our numerical scheme uses the procedure described above and reduces the problem to the summation of a relatively small and time-independent number of terms. This allows us to compute $S^{(2)}(t_1,t_2)$ with minimal numerical effort.

We can justify the numerical procedure separately for two overlapping intervals of t_1 and t_2. In the case $\min(t_1,t_2) \lesssim 1$ the series can be truncated already at $N \sim 10$. At $n \gtrsim 10$ the decay of the terms $F(n;t_1,t_2)$ is exponential, and the remainder is negligible. Therefore, the numerical value of $S^{(2)}$ is obtained by the summation of several terms.

In the case $\min(t_1,t_2)\gtrsim 1$ we are not far from the asymptotic region $t_1,t_2\gg 1$, and $S^{(2)}$ may be found by a simple numerical implementation of the remainder calculation (59). Since we use few terms in the expansion (59) and approximate them by finite differences, the numerical precision is determined by how smoothly the numbers $F(n;t_1,t_2)$ behave as n increases. This is essentially determined by the value of n. The smoothness is only slightly influenced by the values of $t_1,t_2\gtrsim 1$, which can be rationalized by considering the principal asymptotic of $S^{(2)}$ at $t_1,t_2\gg 1$. The series (55) is not purely alternating because of the presence of quasioscillations proportional to $n^{\pm s}=e^{\pm i|s|\ln n}$ in $F(n;t_1,t_2)$. To ensure a sufficiently smooth behavior of $F(n;t_1,t_2)$ at $n>N$ one must choose larger N for larger values of $|s|$.

In practice, a reasonable relative error $\lesssim 10^{-3}$ is achieved if merely $N\sim 10^2$ or fewer terms are retained in the partial sum S_N for $s\sim 5i$ (larger values of $|s|$ would require more terms). In the expansion (59) the third term identically vanishes because $E_2(1)=0$. We use the two first terms in the expansion, and represent the first derivative by the discrete difference with third-order accuracy. Therefore, the neglected contributions scale at best as $O(F_{00}(N;t_1,t_2)e^{-4\min(t_1,t_2)})$. The efficiency of the procedure is remarkable. We need to calculate only around $N\sim 10^2$ terms, which should be compared with a much bigger number $e^{10}>10^4$ at which the summand $F(n;t_1,t_2)$ starts to decay exponentially if $\min(t_1,t_2)\sim 10$. At first sight, a summation of 10^2 terms versus 10^4 terms does not appear to be a crucial improvement, given today's computational capacities. However, the bottleneck here is in computing the individual terms that are represented via the hypergeometric functions. This computational effort grows dramatically for the terms $F(n;t_1,t_2)$ with large n, where the series starts to converge in the absolute sense. Overall, computing a 2D spectroscopic signal with the developed approach requires several minutes of CPU time using such a simple and high-level tool as MATHEMATICA. This qualifies for an "almost analytical" calculation of the complete signal.

In conclusion, we emphasize that only a finite number of the series terms is used in the summation procedure. Thus, the asymptotic expansion of the second-order response function turns out to be determined by the expansions of $A_n(t;s)$ at $t\to\infty$. The latter may be viewed as spectral decompositions of the evolution operator matrix elements. In fact, the strongly chaotic system we consider is characterized by Ruelle-Pollicott resonances $\omega_\nu=\nu+1/2\pm s$. Only even resonances with $\nu=2k$, where $k=0,1,\ldots$, contribute to the spectral decomposition. This result for the second-order response is nontrivial because the expansion can be made only after the summation of the series over angular harmonics. This means that the expansion is only asymptotic.

The convergence issues can be completely avoided by introducing infinitesimal noise. Nonzero noise provides the convergence of the series over angular harmonics for a given pair of resonances [32]. In the limit of the vanishing diffusion coefficient (noise intensity), the terms of the series turn into their noiseless counterparts introduced in Eq. (56). The application of the remainder summation procedure, described above, requires only smoothness of the series terms. Therefore, the sum of the series is determined by a finite number of terms, and the asymptotic expansion appears independent of the vanishing diffusion coefficient. This noise regularization is meaningful, since the way the convergence is enforced is irrelevant for the asymptotic expansion.

VI. NUMERICAL RESULTS

Experimental data on 2D time-domain spectroscopy that probes the response function $S^{(2)}(t_1,t_2)$ are usually presented using a so-called 2D spectrum, which is obtained by a numerical 2D Fourier transform of the response function with respect to t_1 and t_2:

$$S^{(2)}(\omega_1,\omega_2)=\int\int_0^\infty dt_1\,dt_2 e^{i(\omega_1 t_1+\omega_2 t_2)}S^{(2)}(t_1,t_2). \quad (65)$$

To provide a spectroscopic view of chaotic vibrational dynamics, in this section we present some numerical results on 2D spectra for a particular strongly chaotic system studied in this paper.

As we have shown above, the 2D response in our model can be expressed in terms of the properties of the Laplacian eigenmodes that participate in the expansion of the dipole function $f(\boldsymbol{r})$. Since the dipole is generally a smooth function of the system coordinates, the number N_f of relevant eigenmodes is typically small. To study the important features of the signals we consider the second-order response function in the simplest cases $N_f=1$ and 2. The latter represents the simplest situation that involves diagonal and cross peaks in the 2D spectrum. Analytical results for this case, which generalize those of Sec. V, are derived in Appendix E.

In the case $N_f=1$ the second-order response function depends on a spectral parameter s and an additional parameter a_0. Both parameters are expressed in terms of the only Laplacian eigenmode that represents $f(\boldsymbol{r})$ [see Eqs. (43), (54), and (D6)].

For $N_f=2$ we have two spectral parameters s_1 and s_2, and four additional parameters. Similarly to the $N_f=1$ case, all parameters can be expressed in terms of the two relevant Laplacian eigenmodes. As explained at the end of Sec. V C, the parameters can be considered as independent attributes of a particular Riemann surface. For the demonstration of qualitative features, we use a particular choice of the parameters.

The absolute value of the 2D spectroscopic signal $|S^{(2)}(\omega_1,\omega_2)|$ is presented in Fig. 3. Figure 3(a) corresponds to the $N_f=1$ case with the only spectral parameter $s=5i$. Figure 3(b) shows the $N_f=2$ case with two spectral parameters $s_1=5i$ and $s_2=3i$. The real and imaginary components of the 2D spectra are presented in Fig. 4. In the first case we see a diagonal peak with a pronounced stretched feature along ω_1 direction. In the second case we also see cross peaks accompanied by similar stretched features.

Diagonal and off-diagonal peaks are also observed in spectroscopic signals for harmonic and almost harmonic vibrational dynamics. In this case the positions of the peaks are given by the frequencies of the underlying periodic motions, whereas the width is determined by the system-bath interactions and has about the same value in both frequency directions. In the chaotic case the peak positions are determined

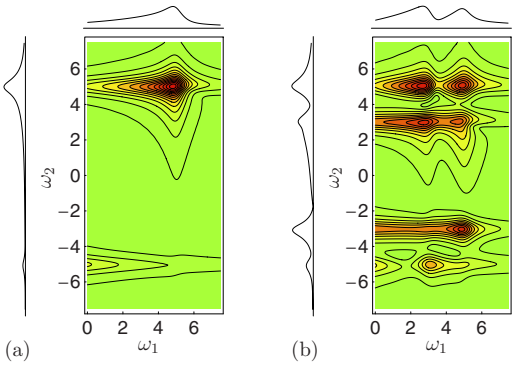

FIG. 3. (Color online) Absolute value of 2D Fourier transform of the second-order response function: (a) single resonance $s=5i$, and (b) linear combination of terms with two resonances $s_1=5i$ and $s_2=3i$. Linear plots show cross sections of the spectra at $\omega_1=\omega_2=5$.

by Ruelle-Pollicott resonances, rather than by the frequencies of some specific periodic orbits. The stretching in spectroscopic signals originates from time-domain damped "breathing" oscillations with a variable period caused by strong nonlinearity of the underlying vibrational dynamics and can be interpreted as a signature of chaos.

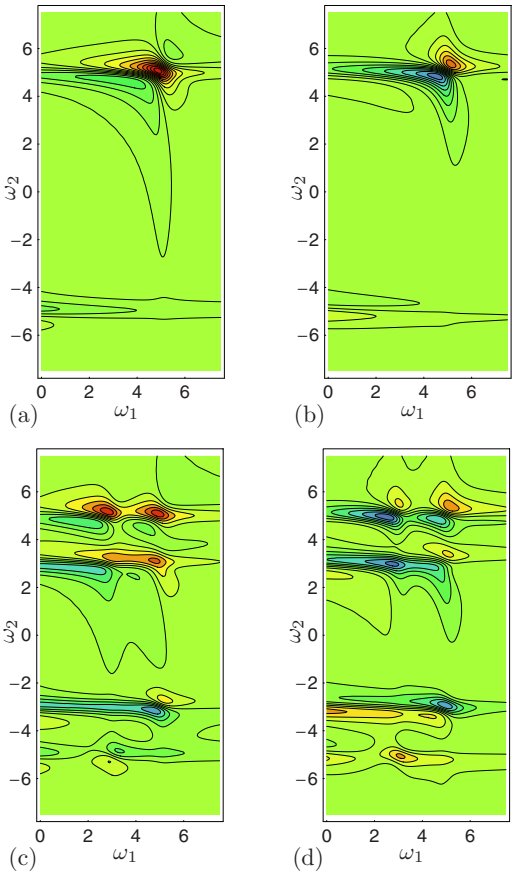

FIG. 4. (Color online) Real and imaginary parts of 2D spectra: (a) real and (b) imaginary part with the single resonance $s=5i$; (c) real and (d) imaginary part of linear combination of terms with two different resonances $s_1=5i$ and $s_2=3i$.

VII. CONCLUSION

Previous studies of the integrable systems revealed the appearance of unphysical divergences in the classical nonlinear response functions at long times. The divergence originates from the linear time growth of stability matrix elements in integrable systems. Legitimate concern has been raised regarding the behavior of nonlinear response in chaotic systems which are characterized by the exponential growth of certain stability matrix elements.

In the present paper we have studied the classical response in a strongly chaotic system. Using the Liouville space representation for classical dynamics, we found that the response functions exhibit damped oscillations with time. The exponential decay is attributed to the uniform hyperbolicity of the strongly chaotic dynamics, which leads to efficient equilibration in phase space.

We described a general semiquantitative picture of response in strongly chaotic (uniformly hyperbolic) systems. The exponential growth of the stability matrices, which can potentially lead to exponential divergence in response functions, was interpreted by using the Liouville space representation of classical mechanics. As a result of evolution, a smooth initial distribution becomes extremely sharp along the stable directions. The second interaction with the driving field involves derivatives of the evolved distribution along the stable directions. This could result in exponentially growing terms in nonlinear response functions. We demonstrated that, due to smoothness of the initial distribution the dangerous terms completely cancel out, and the nonlinear response functions exhibit exponential decay at long times.

To confirm the established semiquantitative picture we performed a calculation of the linear and second-order response for a chaotic model of a free particle on a compact surface with constant negative curvature. The model possesses dynamical symmetry that allows for an exact solution by applying the group representation theory. We found the long-time asymptotic behavior of the linear and second-order response function that has a form of exponentially damped oscillations. Complete asymptotic series obtained in this paper can be viewed as expansions in Ruelle-Pollicott resonances. The expansion of the linear response in RP resonances is in agreement with the earlier results for the two-time correlation functions [22], since the latter are directly related to the linear response via an analog of the FDT.

Our results are not restricted to strongly chaotic systems. A dynamical system of the general type has mixed phase space which includes both chaotic regions and stability islands. Even in such systems, when the true long-time asymptotic decay of correlations is power law rather than exponential, RP resonances may be noticeable, leading to the intermediate asymptotic exponential decay that persists for a very long time [36].

In the following paper [32], we consider Langevin dynamics associated with the model considered here. Spectral decomposition in the corresponding eigenmodes of the Fokker-Planck operator is a stable legitimate procedure. The spectral decomposition in the presence of noise is a converging series. We show that in the limit of vanishing noise the converging series becomes asymptotic and reproduces the

expansion derived in this paper. The asymptotic expansions of the linear and nonlinear response functions can be interpreted as decompositions in RP resonances.

We suggest the application of our results for the interpretation of spectroscopic data. Classical chaos is quite generic for large molecules. Even for a smaller number of nuclear degrees of freedom, e.g., in small systems of hydrogen bonds [44], the shape of the effective potential energy can make the dynamics chaotic. The restricted motion in the regions with negative curvature of the molecular potential can be qualitatively described as free motion on a compact Riemann manifold with negative curvature. Our detailed analysis was focused on the second-order response which is absent in the spectroscopy of the bulk materials. Spectroscopy on the surface [45], in the absence of inversion symmetry, can measure nonvanishing response functions of even order.

When the 2D spectroscopic data are interpreted in terms of the underlying dynamics, the peaks are usually attributed to some periodic motions in the system. We showed that chaotic dynamics can result in similar diagonal and off-diagonal (cross) peaks in spectroscopic signals that should be attributed to RP resonances, and are not related to any specific periodic orbits. Note that the frequencies and decay rates of the RP resonances can be retrieved from the dynamical ζ function that can be represented as a product over all periodic orbits [21]. Stated differently, the RP resonances are related to periodic orbits, yet in an extremely collective way, and may not be attributed to any particular periodic motions. Therefore, they can be referred to as collective chaotic resonances. Our numerical results showed pronounced stretched features associated with diagonal and off-diagonal peaks. These features result from breathing damped oscillations that originate from contributions of multiple RP resonances with similar oscillation frequencies (imaginary parts) and different damping rates (real parts). Breathing oscillations are known to be typical in strongly nonlinear dynamical systems. On the other hand, 2D spectra in harmonic or almost harmonic systems coupled to a multimode harmonic bath usually show similar peak patterns in both frequency directions. We suggest that the stretched versus nonstretched peak shape could be an indicator to distinguish between the collective versus individual nature of resonances in spectroscopic signals.

ACKNOWLEDGMENT

This work was supported by Wayne State University.

APPENDIX A: INTEGRABLE AND ALMOST INTEGRABLE DYNAMICS

The dynamics of a classical Hamiltonian system in the vicinity of an equilibrium (stationary) point can be adequately described by a system of uncoupled harmonic oscillators. This is achieved by expanding the classical Hamiltonian H up to second order in dynamical variables (the first-order terms vanish for an expansion around a stationary point). A harmonic system represents the simplest example of integrable dynamics.

The evolution of integrable systems with n degrees of freedom is naturally described in terms of n canonical pairs of action and angle variables. Action variables c_j with $j=1,\ldots,n$ are first integrals of motion in involution, i.e., $\{H,c_j\}=0$ and $\{c_i,c_j\}=0$. The Hamiltonian $H(\boldsymbol{\eta})=H(c_1,\ldots,c_n)$ depends on the integrals of motion only. Therefore, the corresponding phase-space vector fields (differential operators) $\hat{c}_j=\{c_j,\cdot\}$ commute with each other and describe motions along the tori with frequencies $\omega_j=\partial H(c_1,\ldots,c_n)/\partial c_j$, which parametrically depend on the integrals of motion. Since for given values of the integrals of motion the angular velocities are constant, such dynamics is referred to as conditionally periodic (or quasiperiodic) motion. For the values of the action variables determined by the initial conditions, the trajectories lie on the n-dimensional torus, which is a subspace of $2n$-dimensional phase space. The motion on the torus is strictly periodic if the ratios of the angular velocities are rational (resonant torus); if the angular velocities are incommensurate, the trajectories densely cover the torus (nonresonant torus). Harmonic dynamics is the simplest case of integrable dynamics, when the frequencies ω_i, $i=1,\ldots,n$, are independent of the action variables c_j.

The nonlinear response functions for classical integrable dynamics have been shown to have power law divergence at long times which can be eliminated by invoking a quantum description [8–12]. Divergence of nonlinear response in integrable systems does not imply unphysical behavior by itself, since integrable dynamics is an idealization. In real systems, quantum effects, interactions with the bath, or irregular dynamics may provide a necessary regularization. While the first two phenomena have been discussed in the literature, we concentrate on the last. A small, yet generic, perturbation of the system Hamiltonian destroys integrability. However, such a perturbation does not break down the linear divergence in the response functions. This follows from the qualitative picture of almost integrable dynamics established by the celebrated Kolmogorov-Arnold-Moser (KAM) perturbation theory [15]. The KAM theory states that a sufficiently small perturbation does not destroy most nonresonant tori, which means that in the invariant subspace of the entire phase space represented by the remaining distorted tori the dynamics preserves its quasiperiodic nature. Although motion inside the instability zones (where the tori are destroyed) becomes chaotic, their relative measure in the phase space is small for small perturbations to the integrable dynamics. In the simplest $n=2$ case the zones of instability are confined between remaining invariant tori.

It has been pointed out [9,10] that the divergence of the classical response functions in integrable systems originates from quasiperiodic nature of the underlying motion. Combined with the picture of almost integrable dynamics established by KAM theory, this demonstrates that the unphysical divergence of the response functions is stable with respect to at least weak deviations from integrability.

APPENDIX B: DYNAMICAL SYMMETRY OF GEODESIC FLOWS ON RIEMANN SURFACES WITH CONSTANT NEGATIVE CURVATURE AND REPRESENTATION THEORY

This appendix contains some basic aspects on the geometry of Riemann surfaces with constant negative curvature

that are necessary for employing the SO(2,1) dynamical symmetry [39–42]. This symmetry allows us to decompose the free-particle dynamics using irreducible representations and map the original dynamical problem onto an effective one-dimensional dynamics on a circle.

The fundamental group $\Gamma_g=\pi_1(M_g^2)$ describes noncontractible closed paths on a Riemann surface M_g^2 of genus g. The group Γ_g is generated by $2g$ elements a_j,b_j, where $j=1,\ldots,g$, with the only relation $\Pi_{j=1}^g a_j b_j a_j^{-1} b_j^{-1}=1$. In the case $g>1$ the compact surface is covered $H\to M_g^2$ by the hyperbolic plane H, which can be implemented as a pseudosphere determined by the equation $y_1^2+y_2^2-y_0^2=-1$ with $y_0>0$ embedded in the 3D Minkowski space with a metric $d\ell^2=-dy_0^2+dy_1^2+dy_2^2$ (other well-known equivalent implementations include the Poincaré disk and the upper complex half plane). The fundamental group acts freely in H, so that $M_g^2\cong\Gamma_g\backslash H$. The reduced phase space M_g^3, considered as a bundle $S^1\to M^3\to M^2$, whose fibers are unit velocity or momentum vectors, being pulled back to H, forms a bundle $S^1\to G\to H$, where $G\cong\mathrm{SO}(2,1)$ can be represented as a pseudo-orthogonal group. This can be visualized as follows: $G\cong\mathrm{SO}(2,1)$ consists of points in H (positions) that can be considered as 3D vectors with norm -1 in the Minkowski metric, together with unit velocity vectors that can be interpreted as norm 1 vectors orthogonal to the position vectors (with respect to the Minkowski metric). Extending these two pseudo-orthonormal vectors to a pseudo-orthonormal basis set, we interpret G as the space of pseudo-orthonormal basis sets; the latter can be thought of as the pseudo-orthogonal group SO(2,1). Factorizing $G\cong\mathrm{SO}(2,1)$ with respect to the right action of its maximal compact subgroup $K\cong\mathrm{SO}(2)$ we arrive at $H\cong G/K$. The action of Γ_g in H can be naturally extended to a left action of Γ_g in G, which determines the embedding $\Gamma_g\subset G$. This leads to convenient representations $M_g^2\cong\Gamma_g\backslash G/K$ and $M_g^3\cong\Gamma_g\backslash G$. In particular, this interprets the action of G in M_g^3 as originating from the right action of G in itself.

The presented picture has a very transparent interpretation. We start with a Riemann surface M_g^2 of genus $g>1$ with constant negative scalar curvature $K=-1$. As stated in Sec. IV, we have three canonical vector fields in M_g^3: $\sigma_z=\partial/\partial\theta$, σ_1 which determines the geodesic flow (classical dynamics of a free particle), and $\sigma_2=[\sigma_1,\sigma_z]$. In the case of constant curvature they form the Lie algebra so(2,1) with respect to the vector field commutator. Explicit expressions for the vector fields are presented in Sec. IV and in Appendix C. This defines an action of so(2,1) in M_g^3 that can be naturally extended to $G\to H$, considered as the pullback of $M_g^3\to M_g^2$ to H. The algebra action in G can be integrated to a group action, which implies that locally G has a structure of the universal Lie group associated with the algebra so(2,1). A careful study of the global properties of G shows that in fact $G\cong\mathrm{SO}(2,1)$. This immediately implies that $H\to M_g^2$ is equivalent to SO(2,1)/SO(2) as a Riemann space, i.e., H is the hyperbolic space. This has a very important implication that the local structure of any Riemann surface M_g^2 with constant scalar curvature $K=-1$ is locally equivalent to the hyperbolic space H, whereas M_g^3 is locally equivalent to G. In particular, this implies that all local quantities (e.g., the Laplacian in M_g^2, as well as the Poisson bracket ω and the geodesic flow in M_g^3) can actually be computed in H and G, and afterwards expressed in terms of the canonical vector fields σ_l, $l=1,2,z$. This is a straightforward way to derive Eq. (21).

We also note that for a Riemann surface with $g>1$ and not necessarily constant curvature the metric determines a complex-analytical structure, whereas the universal cover $H\to M_g^2$ is equivalent to the hyperbolic plane and preserves the complex-analytical structure. This implies $M_g^2\cong\Gamma_g\backslash H$. Since the group of conformal diffeomorphisms of H coincides with its isometry group SO(2,1), we have $\Gamma_g\subset G$. This defines a metric in M_g^2 that has constant curvature $K=-1$ and is conformally equivalent to the original metric. Therefore, denoting by $\mathcal{M}_g$ the moduli space of complex analytical structures for genus g, we can describe a Riemann surface with constant curvature $K<0$ by a pair (η,K) with $\eta\in\mathcal{M}_g$.

The representations of M^3 and M^2 in terms of the groups $K,\Gamma\subset G$,

$$M^3\cong\Gamma\backslash G,\quad M^2\cong\Gamma\backslash G/K\cong\Gamma\backslash H\cong M^3/K,$$

$$H\cong G/K \tag{B1}$$

are very convenient for describing invariant integration measures. Since G, K, and Γ are unimodular groups, according to the theorem on invariant measures in homogeneous spaces [40–42], there is a unique invariant measure in $\Gamma\backslash G$ that is locally equivalent (in the sense of covering) to the Haar invariant measure in G. The latter generates an invariant measure in G/K that is locally equivalent to the measure in M^2 generated by the metric. Combined with the main property of invariant measures in homogeneous spaces, this implies

$$\int_{M^3} d\boldsymbol{x}\, g(\boldsymbol{x})=\int_{M^2} d\boldsymbol{r}\int_{K_{\boldsymbol{r}}}\frac{d\theta}{2\pi}g(\boldsymbol{r},\theta) \tag{B2}$$

for any integrable function $g(\boldsymbol{x})$. This measure provides an invariant scalar product in the space $\mathcal{H}$ of functions in M^3. Besides, implementing functions $\tilde{g}(\boldsymbol{r})$ in M^2 as functions $g(\boldsymbol{x})$ in M^3 that do not depend on θ, i.e., $\sigma_z g=0$, we have

$$\int_{M^2} d\boldsymbol{r}\,\tilde{g}(\boldsymbol{r})=\int_{M^3} d\boldsymbol{x}\, g(\boldsymbol{x}). \tag{B3}$$

Therefore, $\mathcal{H}$ can be decomposed into a direct sum of irreducible representations of G,

$$\mathcal{H}=\mathcal{H}^{(0)}\oplus\bigoplus_{s\in\mathrm{Spec}(M^2)}\mathcal{H}_s\oplus\bigoplus_{n\in\mathbb{Z}}^{n\neq 0} m_n\mathcal{H}^{(n)}. \tag{B4}$$

In Eq. (B4) $\mathcal{H}^{(0)}$ denotes the one-dimensional unit representation that represents constant functions, $\mathcal{H}_s$ denote principal series representations [with purely imaginary values of $s\in\mathrm{Spec}_0(M^2)$ where $\mathrm{Im}\, s>0$] and complementary series representations (with real values of $0\le s<1/2$), whereas $\mathcal{H}^{(n)}$ are discrete series representations with the integer factors $m_n\ge 0$ describing how many times a representation participates in the decomposition.

APPENDIX C: ALGEBRA so(2,1) AND THE POISSON BRACKET

In this appendix, we derive a Poisson bracket in the form of Eq. (21). We start with the canonical form of the Poisson bracket in terms of coordinates r^i and conjugated momenta $p_i = \partial L / \partial \dot{r}^i$,

$$\omega = \frac{\partial}{\partial p_i} \otimes \frac{\partial}{\partial r^i} - \frac{\partial}{\partial r^i} \otimes \frac{\partial}{\partial p_i}, \tag{C1}$$

where we imply summation over repeated indices.

We represent the particle momentum in terms of its absolute value ζ and a polar angle θ that determines the momentum direction. The algebra element $\sigma_z = \partial / \partial \theta$ generates rotation of the momentum. The geodesic flow is generated by $\sigma_1 = \hat{L} / \zeta$. The third vector field in the reduced phase space is described by the differential operator

$$\sigma_2 \equiv [\sigma_1, \sigma_2] = E_{in} g^{ik} \left(\frac{\partial \zeta}{\partial p_n} \frac{\partial}{\partial r^k} - \frac{\partial \zeta}{\partial r^k} \frac{\partial}{\partial p_n} \right) + \frac{\partial}{\partial q^k} (E_{in} g^{il} p_l) \left(\frac{\partial \zeta}{\partial p_k} \frac{\partial}{\partial p_n} - \frac{\partial \zeta}{\partial p_n} \frac{\partial}{\partial p_k} \right). \tag{C2}$$

Next, we show that $\sigma_1, \sigma_2, \sigma_z$ form the algebra so(2,1). The coefficients of the first-order linear differential operator $[\sigma_2, \sigma_z]$ include the metric tensor and its first derivatives. A straightforward yet tedious calculation performed in the basis set of four vectors related to the canonical variables p_i, r^i results in the relation $[\sigma_2, \sigma_z] = -\sigma_1$. A similar calculation yields the commutator $[\sigma_1, \sigma_2] = -K(\boldsymbol{r}) \sigma_z$, which contains configuration space curvature $K(\boldsymbol{r})$, and is indeed expressed only through the generator σ_z. In the case of constant negative curvature, the rescaling of σ_1 and σ_2 leads to the so(2,1) commutation relations

$$[\sigma_1, \sigma_2] = \sigma_z, \quad [\sigma_1, \sigma_z] = \sigma_2, \quad [\sigma_2, \sigma_z] = -\sigma_1. \tag{C3}$$

A number of transformations allow us to express the Poisson bracket (C1) in terms of the operators $\partial_\zeta, \sigma_1, \sigma_2, \sigma_z$. The simple form

$$\omega = \frac{\partial}{\partial \zeta} \otimes \sigma_1 - \sigma_1 \otimes \frac{\partial}{\partial \zeta} + \frac{1}{\zeta} (\sigma_2 \otimes \sigma_z - \sigma_z \otimes \sigma_2) \tag{C4}$$

reflects the presence of the dynamical symmetry.

The first two terms of the Poisson bracket determine the phase-space velocity. The constant coefficient in front of the second term can also be deduced from the condition $S^{(2)}(t_1, 0) = 0$.

APPENDIX D: UNITARY IRREDUCIBLE REPRESENTATIONS OF SO(2,1)

In this appendix we describe a convenient implementation of unitary irreducible representation of SO(2,1) in terms of functions on the circle S^1. This provides a mapping of the free-particle dynamics onto a 1D problem. Since the group $G \cong \mathrm{SO}(2,1)$ has a double covering $\mathrm{SL}_2(\mathrm{R}) \to \mathrm{SO}(2,1)$, irreducible representations of G are provided by even irreducible representations of $\mathrm{SL}_2(\mathrm{R})$ (see, e.g., [41]). This situation is conceptually close the the case of irreducible representations of SO(3) given by even, i.e., integer-spin, representations of a double cover $\mathrm{SU}(2) \to \mathrm{SO}(3)$ of SO(3). We can follow the approach of Ref. [41] for $\mathrm{SL}_2(\mathrm{R})$ and translate it to the language convenient for $G \cong \mathrm{SO}(2,1)$.

The space $\mathcal{H}_s$ of an irreducible representation of G that belongs to the principal or complementary series has a convenient basis set Ψ_k of angular harmonics defined by $\sigma_z \Psi_k = ik \Psi_k$. We have the following relations between the basis functions:

$$\sigma_\pm \Psi_k = \left(\pm k + \frac{1}{2} - s \right) \Psi_{k \pm 1}, \quad \sigma_z \Psi_k = ik \Psi_k,$$

$$(\Psi_k, \Psi_{k'}) = 0, \quad \text{for } k \neq k', \tag{D1}$$

where $\sigma_\pm = \sigma_1 \pm i \sigma_2$ are the raising and lowering operators. In the case of imaginary s (principal series) the functions $\Psi_m(u)$ are normalized and represent the normalized functions $\psi_k(\boldsymbol{x}; s)$, i.e.,

$$\int_{M^3} d\boldsymbol{x} [\psi_{k'}(\boldsymbol{x}; s')]^* \psi_k(\boldsymbol{x}; s) = \delta_{k'k} \delta_{s's}, \tag{D2}$$

where $d\boldsymbol{x}$ is the invariant measure in M^3 defined up to a constant [40–42]. We can alternatively view Eq. (D1) as a definition of a so(2,1) representation parametrized by s. In Appendix C we directly verify that the operators σ_1, σ_2, and σ_z satisfy the so(2,1) commutation relations given by Eq. (C3). When the representation space $\mathcal{H}_s$ is implemented as a Hilbert vector space of functions $\Psi(u)$ on a circle, we have

$$\sigma_z = \frac{d}{du}, \quad \sigma_1 = \sin u \frac{d}{du} + \frac{1 - 2s}{2} \cos u,$$

$$\sigma_2 = -\cos u \frac{d}{du} + \frac{1 - 2s}{2} \sin u,$$

$$\sigma_\pm = \exp(\pm iu) \left(\mp i \frac{d}{du} + \frac{1 - 2s}{2} \right), \quad \Psi_k(u) = \exp(iku). \tag{D3}$$

The validity of Eqs. (C3) and (D1) for the generators σ and basis vectors Ψ_k defined by Eqs. (D3) can be verified directly. The generators have a simple form of first-order differential operators because each representation $\mathcal{H}_s$ is induced [40] from a one-dimensional representation (parametrized by s) of a two-dimensional subgroup $AN \subset G$ [41]. It is implemented in the space of functions in the maximal compact subgroup $K \subset G$ where $K \cong \mathrm{SO}(2) \cong S^1$. In the case of imaginary s (principal series) the inducing representation is unitary. Therefore, the induced representation has a natural scalar product [40]

$$(\Psi, \Psi') = \int_0^{2\pi} \frac{du}{2\pi} [\Psi'(u)]^* \Psi(u). \tag{D4}$$

It can be easily verified that the generators σ_l for $l = 1, 2, z$ in the implementation of Eq. (D3) are anti-Hermitian operators with respect to the scalar product defined by Eq. (D4). As

can be seen from Eq. (D4), the set of vectors Ψ_k constitute an orthonormal basis for imaginary s, and the scalar product $(\sigma_+\Psi_0,\sigma_+\Psi_0)=(1-4s^2)/4$ is a positive real number. Besides imaginary s, the scalar product is also positively defined for real s with $-1<2s<1$, which corresponds to the complementary series. In this case, the representations $\mathcal{H}_s$ are not unitary with respect to the scalar product of Eq. (D4); however, another scalar product still diagonal in the basis set of Ψ_k can be defined (this procedure is also known as representation unitarization [41]), so that the representation becomes unitary. We do not use the complementary series representations in the calculation of the response because they lead to the exponential decay without the oscillatory behavior.

Irreducible representations $\mathcal{H}^{(n)}$ of the discrete series can be considered as subrepresentations $\mathcal{H}^{(n)}\subset\mathcal{H}_{n+1}$, and $\mathcal{H}^{(n)}\subset\mathcal{H}_{n-1}$ for $n>0$ and $n<0$, respectively, generated by the vectors Ψ_k with $k\geq n$ and $k\leq n$, respectively, which creates a certain inconvenience. This does not constitute a major problem, since the discrete representations $\mathcal{H}^{(n)}$ can be alternatively holomorphically induced from unitary representations of the maximal compact subgroup $K\cong \mathrm{SO}(2)$. We are not discussing this construction here, since discrete representations do not contain the zero-momentum state Ψ_0 and, therefore, they do not contribute to the linear and second-order response.

It is also important to note that irreducible representations of the principal and complementary series characterized by opposite values of s are unitarily equivalent, i.e., $\mathcal{H}_{-s}\cong\mathcal{H}_s$, which follows from the fact that the representation unitarization is determined by the value of s^2 [41]. For the principal series representations this property is clearly seen from Eq. (D1). The latter implies that in the case of imaginary s the vectors $(\sigma_\pm)^k\Psi_0$ for opposite values of s are only different by phase factors and can be connected by a unitary transformation that is diagonal in the Ψ_k basis set. The purpose of the unitary transformation is to compensate the aforementioned phase factors. In particular, this justifies the agreement that the spectrum $\mathrm{Spec}(M^2)$ contains only imaginary s with $\mathrm{Im}\, s>0$ and real s with $0\leq s<1/2$.

We conclude this appendix by relating the spectrum $\mathrm{Spec}(M^2)$ to the spectrum of the Laplacian in M^2. To that end we introduce the Casimir operator $\hat{C}$ that commutes with all so(2,1) generators, and, therefore, is a constant in any irreducible representation due to the Shur lemma:

$$\hat{C}=-\frac{1}{2}(\sigma_+\sigma_-+\sigma_-\sigma_+)+(\sigma_z)^2,$$

$$[\hat{C},\sigma_l]=0 \quad \text{for } l=1,2,z, \quad \hat{C}\Psi=\frac{1-4s^2}{4}\Psi \quad \text{for } \Psi\in\mathcal{H}_s, \tag{D5}$$

where we used the ladder operators $\sigma_\pm$. We can further interpret functions in M^2 as functions $f(\boldsymbol{x})$ in M^3 independent of the momentum direction θ, i.e., $\sigma_z f=0$. It is one of the signatures of the dynamical symmetry that, if acting on functions in M^2, the Laplacian operator (which is proportional to the Hamiltonian of a free quantum particle) is expressed in terms of the Casimir operator as

$$-\nabla^2=-\frac{1}{2}(\sigma_+\sigma_-+\sigma_-\sigma_+)=\hat{C}-(\sigma_z)^2,$$

$$\nabla^2\psi_0(\boldsymbol{x};s)=-\frac{1-4s^2}{4}\psi_0(\boldsymbol{x};s). \tag{D6}$$

Here ∇^2 stands for the Laplacian. It follows from Eq. (D6) that the spectrum $\mathrm{Spec}(M^2)$ of a Riemann surface is totally determined by the spectrum of the Laplacian. On a compact surface, the spectrum of the Laplacian is discrete, and the eigenvalues are negative. The functions $\psi_k(\boldsymbol{x};s)$ with $s\in\mathrm{Spec}_0(M^2)$ can be expressed in terms of the Laplacian eigenfunctions $\psi_0(\boldsymbol{x};s)$ by using (28). For the sake of completeness, we note that the functions $\psi_k(\boldsymbol{x};s)$ for $s\in\mathrm{Spec}(M^2)$ (known as modular forms of degree k; see Ref. [41]) are also eigenmodes of the Laplacian. The Laplacian operator can be viewed as the quantum Hamiltonian of a free particle moving in a homogeneous magnetic field whose intensity is proportional to k.

Given the function $\Psi(u)$ on the circle, one can find its counterpart $\psi(\boldsymbol{x};s)$ in the representation space $\mathcal{H}_s$:

$$\psi(\boldsymbol{x};s)=\sum_{k=-\infty}^{\infty}\int_{-\pi}^{\pi}du\ e^{-iku}\Psi(u)\psi_k(\boldsymbol{x};s), \tag{D7}$$

where $\psi_k(\boldsymbol{x};s)$ are basis functions in $\mathcal{H}_s$.

APPENDIX E: MATRIX ELEMENTS IN THE SECOND-ORDER RESPONSE FUNCTION

This appendix includes some details necessary for the calculation of the second-order response when the dipole f contains contributions from different representations of the principal series. We start with the analysis of the geometrical ingredients referred to as matrix elements.

In Sec. V B we have derived the recurrence relations for the matrix elements in the simplest case of a single representation labeled by an imaginary number s. Since ψ_0 is a real-valued function (see Sec. II), we have $a_1=a_{-1}=a_0/2$. The recurrence relation (52) is symmetric with respect to the sign reversal of k, and we conclude that $a_{-k}=a_k$. Therefore, all terms a_k and b_k are determined by a single real number a_0. Another way to come to the conclusion is to notice that

$$\psi_n^*(\boldsymbol{x},s)=\frac{\Gamma\left(n+\frac{1}{2}-s\right)\Gamma\left(\frac{1}{2}+s\right)}{\Gamma\left(n+\frac{1}{2}+s\right)\Gamma\left(\frac{1}{2}-s\right)}\psi_{-n}(\boldsymbol{x},s). \tag{E1}$$

Next we calculate the coefficients involved in the second-order response in a general situation when the coupling f includes contributions from several irreducible representations characterized by imaginary numbers $s_1,s_2,\ldots$. In this case the coefficients are labeled by additional indices:

$$a_k^{qrs}=\int d\boldsymbol{x}\ \psi_k^*(\boldsymbol{x};q)\psi_0(\boldsymbol{x};r)\psi_k(\boldsymbol{x};s), \tag{E2}$$

$$b_k^{qrs} = 2\int d\boldsymbol{x}\ \psi_k^*(\boldsymbol{x};q)\sigma_+\psi_0(\boldsymbol{x};r)\psi_{k-1}(\boldsymbol{x};s). \tag{E3}$$

Choosing the zero-momentum eigenfunctions $\psi_0^*(\boldsymbol{x};q)$ to be real, we see that a_0^{qrs} remains invariant under permutations in $\{q,r,s\}$. Employing Eqs. (D1) we can generalize the recurrence relations (52):

$$\begin{aligned}(2k+1+2q)(2k+1-2s)a_{k+1}^{qrs} &= -(2k-1-2q)(2k-1+2s)a_{k-1}^{qrs} \\ &\quad + (8k^2+1-4q^2+4r^2-4s^2)a_k^{qrs},\end{aligned} \tag{E4}$$

$$b_{k+1}^{qrs} = (2k+1-2q)a_k^{qrs} - (2k+1-2s)a_{k+1}^{qrs}. \tag{E5}$$

This is done similarly to the special case $q=r=s$ described above. The asymptotic form that generalizes a leading term in Eq. (F1) consists of two contributions:

$$a_k^{qrs} \propto k^{-1/2-q+s\pm r}. \tag{E6}$$

The numerical results of Sec. VI are presented for the case of two terms (two representations) in the expansion (30) of the dipole moment f. This is the simplest case that involves cross peaks in 2D spectroscopic signals. We obtain the second-order response in a form similar to Eq. (53):

$$\begin{aligned}S^{(2)} = \int d\zeta \frac{\partial\rho_0}{\partial E}\frac{\partial}{\partial t_1}\sum_{p,q,r=s_1,s_2} B_pB_qB_r\sum_{n=0}^{\infty}(-1)^n \\ \times\left\{\left[\left(n+\frac{1}{2}+r\right)a_n^{pqr} - \left(n+\frac{1}{2}+p\right)a_{n+1}^{pqr}\right]\left(t_2\frac{\partial}{\partial t_2}-n\right)\right. \\ \times(A_n^*(t_2;p)A_{n+1}(t_1;r)) \\ -\left[\left(n+\frac{1}{2}-p\right)a_n^{pqr} - \left(n+\frac{1}{2}-r\right)a_{n+1}^{pqr}\right] \\ \left.\times\left(t_2\frac{\partial}{\partial t_2}+n+1\right)[A_{n+1}^*(t_2;p)A_n(t_1;r)]\right\}.\end{aligned} \tag{E7}$$

Since q, r, s adopt only two values s_1 and s_2, the matrix elements a_k turn out to be symmetric, $a_k^{qrs}=a_{-k}^{qrs}$, and Eqs. (E4) at $k=0$ allow us to express a_1^{qrs} via a_0^{qrs}. Since the zero harmonics $\psi_0(\boldsymbol{x};s)$ are real, the coefficients a_0^{qrs} are also real and invariant under any permutation of q, r, and s. Therefore, all matrix elements a_k^{qrs} are divided into four groups and expressed through only four real numbers $a_0^{s_1s_1s_1}$, $a_0^{s_2s_2s_2}$, $a_0^{s_1s_1s_2}$, and $a_0^{s_1s_2s_2}$.

The properties of the sequences $\{a_k^{s_1s_1s_1}\}$ and $\{a_k^{s_2s_2s_2}\}$ have been described above. The conditions necessary to express all numbers in these sets via the terms at $k=0$ are given by $a_1^{sss}=a_0^{sss}/2$.

The third group of matrix elements includes $a_k^{s_1s_1s_2}$, $a_k^{s_1s_2s_1}$, and $a_k^{s_2s_1s_1}$. We express all these matrix elements via $a_0^{s_1s_1s_2}$ using the following relations:

$$a_k^{s_1s_1s_2} = (a_k^{s_2s_1s_1})^*, \quad a_1^{s_1s_2s_1} = \frac{1+4s_2^2-4s_1^2}{2(1-4s_1^2)}a_0^{s_1s_1s_2}, \tag{E8}$$

$$a_1^{s_2s_1s_1} = \frac{1-2s_2}{2(1-2s_1)}a_0^{s_1s_1s_2}. \tag{E9}$$

The fourth group of matrix elements includes $a_k^{s_2s_2s_1}$, $a_k^{s_2s_1s_2}$, and $a_k^{s_1s_2s_2}$, which obey the relations similar to those for the third group but with s_1 and s_2 interchanged. Thus they are expressed in terms of a single real number $a_0^{s_2s_2s_1}$.

We assume the four numbers $a_0^{s_1s_1s_1}$, $a_0^{s_2s_2s_2}$, $a_0^{s_1s_1s_2}$, and $a_0^{s_1s_2s_2}$ to be independent. This is rationalized in a detailed discussion at the end of Sec. V B.

APPENDIX F: ASYMPTOTIC EXPANSION

In this appendix we present some details of the derivation of the asymptotic expansion given by Eq. (63).

First of all, the derivation is based on the assumption that the the terms $F(n)$ in our series can be represented by some smooth function $F(z)$. This is true for the coefficients A_n, which enter Eq. (53), due to their explicit form given by Eq. (38). However, the matrix elements a_n, which also appear in Eq. (53), are given as a discrete set according to Eq. (52). To show that a_k can be represented by a smooth function $a(z)$, we note that, since a_k is a solution of a recurrence relation, its behavior at $k\to\infty$ can be readily analyzed, which results in an expansion

$$a_k = k^{-1/2+s}\sum_{m=0}^{\infty}\frac{\tilde{a}_{m,s}}{k^m} + k^{-1/2-s}\sum_{m=0}^{\infty}\frac{\tilde{a}_{m,-s}}{k^m}. \tag{F1}$$

This yields an analytical function $a(z)$ in a form of an analytical expansion

$$a(z) = z^{-1/2+s}\sum_{m=0}^{\infty}\frac{\tilde{a}_{m,s}}{z^m} + z^{-1/2-s}\sum_{m=0}^{\infty}\frac{\tilde{a}_{m,-s}}{z^m} \tag{F2}$$

in powers of $1/z$ at $z=\infty$.

So far we have demonstrated that the terms $F(k)$ in our series are represented by an analytical function $F(z)$, and therefore the approach for calculating the asymptotic expansion introduced in Sec. V C is in principle legitimate. However, this is not enough yet, since the asymptotic expansion coefficients $S_{m_1m_2}^{(2)}$ involve the derivatives $\partial_z^m F_{m_1m_2}(z)$ at integer $z=k$ values of the argument, as prescribed by Eq. (62). Apparently, it requires explicit knowledge of the analytical function $F(z)$. However, what we really need as a good enough approximation for the derivatives in Eq. (62) so that the neglected terms vanish in the limit $N\to\infty$. This can be achieved by implementing a very simple scheme. For an analytical function $F(z)$, let $F_m^{(k)}(N)$ be an mth-order approximation for its derivative $\partial_z^k F(z)|_{z=N}$ at $z=N$. Then the derivatives $\partial_N^k F_{m_1m_2}(N)$ in Eq. (62) can be safely replaced by their approximate values $F_{m,m_1m_2}^{(k)}(N)$, provided m is large enough. The approximate derivatives can be linearly expressed in terms of the series terms $F(n)$ by solving an obvious system of linear equations

$$\sum_{l=0}^{m}\frac{n^l}{l!}F_m^{(l)}(N) = F(N+n), \quad n=0,\ldots,m. \tag{F3}$$

In the remainder of this appendix we show how to control the neglected terms in the derivation of the asymptotic series. We start by noting that the asymptotic expansion of Eq. (63) should be understood in such a way that for any pair (M_1,M_2) of positive integers we have

$$S^{(2)}(t_1,t_2) = \sum_{m_1=0}^{M_1} \sum_{m_2=0}^{M_2} S^{(2)}_{m_1 m_2}(t_1,t_2) e^{-2(m_1 t_1 + m_2 t_2)} + o(e^{-2(M_1 t_1 + M_2 t_2)}). \quad \text{(F4)}$$

Full control over the neglected terms can be achieved by a proper choice of the intermediate $N(t_1,t_2)$ as a function of $t_1,t_2 \to \infty$ and n in Eq. (61). Note that both $N(t_1,t_2)$ and n also depend on M_1 and M_2. We choose

$$N(t_1,t_2) = \exp[\gamma \min(t_1,t_2)], \quad \text{(F5)}$$

so that for small enough γ we have $1 \ll N \ll e^{t_1}, e^{t_2}$ and hence can expand $F(n;t_1,t_2)$ for $n \leq N$ in powers of e^{-2t_1} and e^{-2t_2} according to Eq. (56). If we keep the terms up to the degree (M_1,M_2), the neglected terms can be estimated as $\sim N^{2(M_1+M_2)+r} \exp[-2 \min(t_1,t_2)] e^{-2(M_1 t_1 + M_2 t_2)}$, where $r=3$ corresponds to a very loose estimate. By choosing γ to be small enough, specifically $[2(M_1+M_2)+r]\gamma < 2$, the neglected terms are $o(e^{-2(M_1 t_1 + M_2 t_2)})$ and can be safely omitted. Finally, no matter how small γ is, we can always find M to be large enough (and independent of t_1 and t_2), so that $N^{-M}(t_1,t_2) = o(e^{-2(M_1 t_1 + M_2 t_2)})$, and the terms omitted in Eq. (62) can also be safely neglected.

[1] A. Tokmakoff, M. J. Lang, D. S. Larsen, G. R. Fleming, V. Chernyak, and S. Mukamel, Phys. Rev. Lett. **79**, 2702 (1997).
[2] M. C. Asplund, M. T. Zanni, and R. M. Hochstrasser, Proc. Natl. Acad. Sci. U.S.A. **97**, 8219 (2000).
[3] M. D. Fayer, Annu. Rev. Phys. Chem. **52**, 315 (2001).
[4] D. M. Jonas, Annu. Rev. Phys. Chem. **54**, 425 (2003).
[5] A. Stolow and D. M. Jonas, Science **305**, 1575 (2004).
[6] J. B. Asbury, T. Steinel, K. Kwak, S. A. Corcelli, C. P. Lawrence, J. L. Skinner, and M. D. Fayer, J. Chem. Phys. **121**, 12431 (2004).
[7] J. M. Gomez Llorente and E. Pollak, Annu. Rev. Phys. Chem. **43**, 91 (1992).
[8] J. A. Leegwater and S. Mukamel, J. Chem. Phys. **102**, 2365 (1995).
[9] W. G. Noid, G. S. Ezra, and R. F. Loring, J. Phys. Chem. B **108**, 6536 (2004).
[10] M. Kryvohuz and J. Cao, Phys. Rev. Lett. **95**, 180405 (2005); J. Chem. Phys. **122**, 024109 (2005).
[11] W. G. Noid and R. F. Loring, J. Chem. Phys. **122**, 174507 (2005).
[12] M. Kryvohuz and J. Cao, Phys. Rev. Lett. **96**, 030403 (2006).
[13] A. Goj and R. F. Loring, J. Chem. Phys. **124**, 194101 (2006).
[14] M. C. Gutzwiller, *Chaos in Classical and Quantum Mechanics* (Springer-Verlag, Berlin, 1990).
[15] V. I. Arnold, *Mathematical Methods of Classical Mechanics* (Springer-Verlag, Berlin, 1989).
[16] P. Gaspard, *Chaos, Scattering, and Statistical Mechanics* (Cambridge University Press, Cambridge, UK, 1998).
[17] P. Cvitanović, R. Artuso, R. Mainieri, G. Tanner, and G. Vattay, *Chaos: Classical and Quantum* (Niels Bohr Institute Press, Copenhagen, 2005).
[18] J. M. Gomez Llorente, H. S. Taylor, and E. Pollak, Phys. Rev. Lett. **62**, 2096 (1989).
[19] N. van Kampen, Phys. Norv. **5**, 279 (1971).
[20] M. Pollicott, Invent. Math. **81**, 413 (1985); **85**, 147 (1986).
[21] D. Ruelle, Phys. Rev. Lett. **56**, 405 (1986).
[22] S. Roberts and B. Muzykantskii, J. Phys. A **33**, 8953 (2000).
[23] S. Mukamel, V. Khidekel, and V. Chernyak, Phys. Rev. E **53**, R1 (1996).
[24] G. Boffetta, G. Lacorata, S. Musacchio, and A. Vulpiani, Chaos **13**, 806 (2003).
[25] M. Falcioni, S. Isola, and A. Vulpiani, Phys. Lett. A **144**, 341 (1990).
[26] D. Ruelle, Phys. Lett. A **245**, 220 (1998).
[27] U. M. B. Marconi, A. Puglisi, L. Rondoni, and A. Vulpiani, e-print arXiv:0803.0719, Phys. Rep. (to be published).
[28] S. Mukamel, *Principles of Nonlinear Optical Spectroscopy* (Oxford University Press, New York, 1995).
[29] C. Dellago and S. Mukamel, Phys. Rev. E **67**, 035205(R) (2003); J. Chem. Phys. **119**, 9344 (2003).
[30] D. J. Evans and G. P. Morriss, *Statistical Mechanics of Nonequilibrium Liquids* (Academic, London, 1990).
[31] S. V. Malinin and V. Y. Chernyak, Phys. Rev. E **77**, 025201(R) (2008).
[32] S. V. Malinin and V. Y. Chernyak, following paper, Phys. Rev. E **77**, 056202 (2008).
[33] L. Barreira and Ya. Pesin, *Nonuniform Hyperbolicity: Dynamics of Systems with Nonzero Lyapunov Exponents* in Encyclopedia of Mathematics and Its Applications (Cambridge University Press, Cambridge, UK, 2007).
[34] F. Vivaldi, G. Casati, and I. Guarneri, Phys. Rev. Lett. **51**, 727 (1983).
[35] C. Dellago and H. A. Posch, Phys. Rev. E **55**, R9 (1997).
[36] S. Fishman and S. Rahav, in *Dynamics of Dissipation*, edited by P. Garbaczewski and R. Olkiewicz, Lecture Notes in Physics Vol. 597 (Springer-Verlag, Berlin, 2002), p. 165.
[37] L. Casetti, C. Clementi, and M. Pettini, Phys. Rev. E **54**, 5969 (1996).
[38] Y. G. Sinai, Russ. Math. Surv. **25**, 137 (1970).
[39] N. L. Balazs and A. Voros, Phys. Rep. **143**, 109 (1986).
[40] A. A. Kirillov, *Elements of the Theory of Representation of Groups* (Springer-Verlag, Berlin, 1986).
[41] S. Lang, $SL_2(R)$ (Addison-Wesley, Reading, MA, 1975).
[42] F. L. Williams, *Lectures on the Spectrum of* $L^2(\Gamma\backslash G)$, Pitman Research Notes in Mathematics (Longman House, London, 1990), Vol. 242.
[43] *Handbook of Mathematical Functions*, edited by M. Abramowitz and I. A. Stegun (Dover, New York, 1972).
[44] J. D. Eaves, J. J. Loparo, C. J. Fecko, S. T. Roberts, A. Tokmakoff, and P. L. Geissler, Proc. Natl. Acad. Sci. U.S.A. **102**, 13019 (2005).
[45] A. Ulman, Chem. Rev. (Washington, D.C.) **96**, 1533 (1996).